https://doi.org/10.5194/acp-2019-592
Preprint. Discussion started: 4 July 2019

Atmospheric Chemistry and Physics Discussions

Simulating age of air and distribution of SF_6 in the stratosphere with SILAM model

Rostislav Kouznetsov[1,2], Mikhail Sofiev[1], Julius Vira[1,3], and Gabriele Stiller[4]

[1]Finnish Meteorological Institute, Helsinki, Finland
[2]Obukhov Institute for Atmospheric Physics, Moscow, Russia
[3]Currently at Cornell University, Ithaca, NY, USA
[4]Karlsruhe Institute of Technology, Karlsruhe, Germany

Correspondence: Rostislav Kouznetsov (Rostislav.Kouznetsov@fmi.fi)

Abstract. The paper presents a comparative study of age of air (AoA) derived with several approaches: a widely used passive tracer accumulation method, the SF_6 accumulation, and a direct calculation of an "ideal age" tracer. The simulations have been performed with the Eulerian chemistry transport model SILAM driven with the ERA-Interim reanalysis for 1980-2018.

The Eulerian environment allowed for simultaneous application of several approaches within the same simulation, and interpretation of the obtained differences. A series of sensitivity simulations revealed the role of the vertical profile of turbulent diffusion in the stratosphere, destruction of SF_6 in the mesosphere, as well as the effect of gravitational separation of gases with strongly different molar masses.

The simulations reproduced well the main features of the SF_6 distribution in the atmosphere retrieved from the MIPAS satellite instrument. It was shown that the apparent very old air in the upper stratosphere derived from the SF_6 profile observations is a result of destruction and gravitational separation of this gas in the upper stratosphere and mesosphere. The effect of these processes add over 4 years to the actual AoA, which, according to our calculations, does not exceed 6-6.5 years.

The destruction of SF_6 and varying rate of emission make it unsuitable to reliably derive AoA or its trends. However, observations of SF_6 provide a very useful means for validation of stratospheric circulation in a model with properly implemented SF_6 loss.

1 Introduction

AoA is defined as the time spent by an air parcel in the stratosphere since its entry across the tropopause (Li and Waugh, 1999; Waugh, 2002). The distribution of the age of air (AoA) is controlled by the global atmospheric circulations, first of all, the Brewer-Dobson and the polar circulation. In particular, the temporal variation of AoA has been used as an indicator of long-term changes in the stratospheric circulation (Engel et al., 2009; Waugh, 2009). AoA has been extensively used to evaluate and compare general circulation and chemical transport models in the stratosphere (Waugh, 2002; Engel et al., 2009).

Simulations of the AoA according to the definition above have been performed with Lagrangian transport models (Eluszkiewicz et al., 2000; Waugh, 2002; Diallo et al., 2012). The trajectories are initiated with positions distributed in the stratosphere and integrated backwards until they cross the tropopause. The time elapsed since the initialization is attributed as age of air at the

https://doi.org/10.5194/acp-2019-592
Preprint. Discussion started: 4 July 2019

Atmospheric Chemistry and Physics Discussions

point of initialization. Moreover, the distribution of the ages of particles originating from some location can be used to get the age spectrum there.

The Eulerian simulations of AoA can be formulated in several different ways. The approaches with an accumulating tracer, mimicking the above-mentioned observational method were used in a comprehensive study by Krol et al. (2018) and several studies before (e.g. Eluszkiewicz et al., 2000; Monge-Sanz et al., 2012). Besides that, a special tracer that presents an analogy of Lagrangian clock has been used. The tracer appears in literature under names "clock-type tracer"(Monge-Sanz et al., 2012) or "ideal age" (Waugh, 2002). The ideal age has constant rate of increasing of mixing ratio everywhere, except for the surface where it is continuously forced to zero. Similar tracers have been long used to simulate age of oceanic water (e.g. England, 1995; Thiele and Sarmiento, 1990).

Direct observations of the age of air, as it is defined above, are not possible, therefore AoA is usually derived from observed mixing ratios of various tracers. The tracers belong to one of two types: various tracers with known tropospheric mixing ratios and lifetimes (Bhandari et al., 1966; Koch and Rind, 1998; Jacob et al., 1997; Patra et al., 2011), and long-living tracers with known trends in tropospheric mixing ratios. The studies published to-date used carbon dioxide CO_2 (Remsberg, 2015), nitrous oxide N_2O (Boering et al., 1996; Andrews et al., 2001), sulphur hexafluoride SF_6 Waugh (2009); Stiller et al. (2012), methane CH_4 (Remsberg, 2015), and various fluorocarbons (Leedham Elvidge et al., 2018).

For accumulating tracers a mean AoA at some point in the stratosphere is calculated as a lag between the times when a certain mixing ratio is observed near the surface and at that point. The lag time is equivalent to the mean AoA defined above only in the case of a strictly linear growth and uniform distribution of the tracer in the troposphere (Hall and Plumb, 1994).

In reality, there is no tracer whose mixing ratio in the troposphere grows strictly linearly. The violation of assumption of the linear growth leads to biases in the resulting AoA distribution and its trends. It has been pointed out that increasing growth rates of CO_2 and SF_6 lead to low-bias of AoA and its trends, and make these tracers ambiguous proxies for AoA (Garcia et al., 2011). Various corrections have been applied in several studies (Hall and Plumb, 1994; Waugh, 2002; Engel et al., 2009; Stiller et al., 2012; Leedham Elvidge et al., 2018) to deduce the "true" AoA from observations of tracers with increasing growth rates. The effect of the correction method on AoA estimates has not been investigated and must be considered as source of uncertainty in resulting estimates (Garcia et al., 2011). Garcia et al. (2011) further conclude that accounting for the biases in trend estimates due to varying growth rates would likely require uniform and continuous knowledge of the evolution of trace species, which is not available from any existing observational dataset. Recently Leedham Elvidge et al. (2018) have shown a minor sensitivity of AoA to the choice of particular correction method, however without detailed analysis of assumptions behind these methods.

Another major source of uncertainty in observational AoA is violation of conservation of a tracer due to sources and sinks, such as oxidation of carbon monoxide and methane for CO_2, or mesospheric destruction for SF_6. The mesospheric sink of SF_6 leads to an "over-aging", especially pronounced in the area of polar vortices. The magnitude of the over-aging was estimated as 2 or more years Waugh (2002). .

The simulations of SF_6 and AoA in the atmosphere with WACCM model (Kovács et al., 2017) have reproduced the effect of over-aging, but of much smaller magnitude than if inferred from SF_6 retrievals from the limb-viewing **MIPAS** instrument

https://doi.org/10.5194/acp-2019-592
Preprint. Discussion started: 4 July 2019

Atmospheric Chemistry and Physics Discussions

operated on-board of the Envisat satellite in 2002-2012 (Stiller et al., 2012), and *in-situ* observations from the ER-2 aircraft (Hall et al., 1999). Kovács et al. (2017) offered two possible scenarios for the discrepancy: either SF_6 loss is still underestimated in WACCM, or MIPAS SF_6 is low biased above $\sim 20\,\mathrm{km}$. Neither of the scenarios have been analysed in depth so far, which leaves the status of MIPAS, the richest to date observational dataset for the stratospheric SF_6, unclear.

The aim of the present study is to provide consistent simulations simultaneously reproducing the spatio-temporal distribution of AoA and the SF_6 mixing ratio in the stratosphere during last 39 years.

With these simulations we

- compare different methods of estimating the AoA and quantify inconsistencies in AoA and its trends arising from violations of the underlying assumptions behind each method
- analyze the causes of the discrepancies in the upper stratosphere between different methods of deriving the AoA
- provide a solid basis for further studies of stratospheric circulation with observations of various trace gases and for studies of climate effects of SF_6

The paper is organized as follows. Sec. 2 gives an overview of the modelling tools, and the modelling and observational data used for the study. Sec. 3 describes the developments made for Silam in order to perform the simulations: vertical eddy diffusivity parametrisation in stratosphere and lower mesosphere, and SF_6 destruction parametrization, as well as the modelling setup. The sensitivity tests and evaluation of the simulations against MIPAS satellite retrievals, and stratospheric-balloon measurements of SF_6 mixing ratios are given in Sec. 4. Sensitivity of AoA and its trends to the choice of the simulation setup and AoA proxy is studied in Sec. 5. The findings of the whole study are summarised in Sec. 6.

2 Methods and input data

2.1 SILAM model

SILAM (System for Integrated modeLling of Atmospheric coMposition) is an off-line chemical-transport model. SILAM features a mass-conservative and positive-definite advection scheme that makes the model suitable for long-term runs (Sofiev et al., 2015). The model can be run at a range of resolutions starting from a kilometer scale in limited-area or in global mode. The vertical structure of modelling domain consist of stacked layers starting from the surface. The layers can be defined either in z- or hybrid sigma-pressure coordinates. The model can be driven with a variety of NWP- (numerical weather prediction) or climate models.

In order to accurately model the AoA and needed tracers, the vertical diffusion part of the transport scheme of SILAM has been refined to account for gravitational separation. In addition, several tracers with specific transformation procedures have been implemented into the model. The specific setup used for the present study is described in Sec. 3.5

https://doi.org/10.5194/acp-2019-592
Preprint. Discussion started: 4 July 2019

Atmospheric Chemistry and Physics Discussions

2.2 ECMWF ERA-interim reanalysis

The ERA-Interim reanalysis from the European Centre for Medium-range Weather Forecasts (ECMWF) had been used as a meteorological driver for our simulations. The data set has T255 spectral resolution and covers the whole atmosphere with 60 hybrid sigma-pressure levels (Dee et al., 2011), having the uppermost layer from 20 to 0 Pa with nominal pressure of 10 Pa. The reanalysis uses a 12-h data assimilation cycle, and the forecasts are stored with a 3-hour time step. We used the fields retrieved form the ECMWF's MARS archive on a lat-lon grid 500x250 points with step of 0.72 degrees. The four forecast times (+3h, +6h, +9 h and +12h) were used from every assimilation cycle to obtain a continuous dataset with 3-hour time step. To drive the dispersion model, the data for 1980-2015 were used.

The ERA-interim reanalysis has been used earlier for Lagrangian simulations of AoA (Diallo et al., 2012) and found to provide ages that agree with those inferred from in-situ observations in the lower stratosphere.

2.3 MIPAS observations of SF_6

To evaluate the results of SF_6 modelling we used the data from the MIPAS instrument operated on-board of Envisat satellite in 2002-2012. MIPAS was a limb-sounding Fourier transform spectrometer with a high spectral resolution measuring in the infrared. Due to its limb geometry, a good vertical resolution of the derived trace gas profiles and a high sensitivity to low-abundant species around the tangent point has been achieved. Along the orbit path, MIPAS measured a profile of atmospheric radiances about every $400\,\mathrm{km}$ with an altitude coverage, in its nominal mode, of about $6 - 70\,\mathrm{km}$ altitude. The vertical sampling was $1.5\,\mathrm{km}$ in the lower part of the stratosphere (up to $32\,\mathrm{km}$) and $3\,\mathrm{km}$ above, with a vertical field of view covering $3\,\mathrm{km}$ at the tangent point. Over a day, about 1300 profiles along 14.4 orbits were measured, covering all latitudes up to the poles at sunlit and dark conditions. The vertical distributions of trace gases were derived from the radiance profiles by an inversion procedure, fitting simulated spectra to the measured ones while varying the atmospheric state parameters.

The retrieval of SF_6 is based on the spectral signature of this species in the vicinity of $10.55\,\mu\mathrm{m}$ wavelength and is in principle described in Stiller et al. (2008, 2012); Haenel et al. (2015). In this study here, we use an updated version of SF_6 data (compared to the one described in Haenel et al. (2015)) called V5H/R_SF6_21/224/225; the absorption cross-section data on SF_6 and a new CFC-11 band in the vicinity of the SF_6 signature provided by J. Harrison (pers. communication) has been used instead of the older cross section data by Varanasi et al. (1994). The updated version provides considerably higher SF_6 mixing ratios in the upper part of the stratosphere (above $30\,\mathrm{km}$) than the versions before and is closer to independent reference data.

The retrieved profiles are sampled on an altitude grid spaced at $1\,\mathrm{km}$, where as the actual resolution of the profiles is between 4 and $10\,\mathrm{km}$ for altitudes below $30\,\mathrm{km}$. The retrievals are supplemented with averaging kernels and error covariance matrices describing uncertainties due to measurement noise, which is normally in the order of 10% of the retrieved value, and the correlations among the retrieved quantities. The error is uncorrelated between profiles, so, averaging makes it negligible in monthly zonal means.

https://doi.org/10.5194/acp-2019-592
Preprint. Discussion started: 4 July 2019

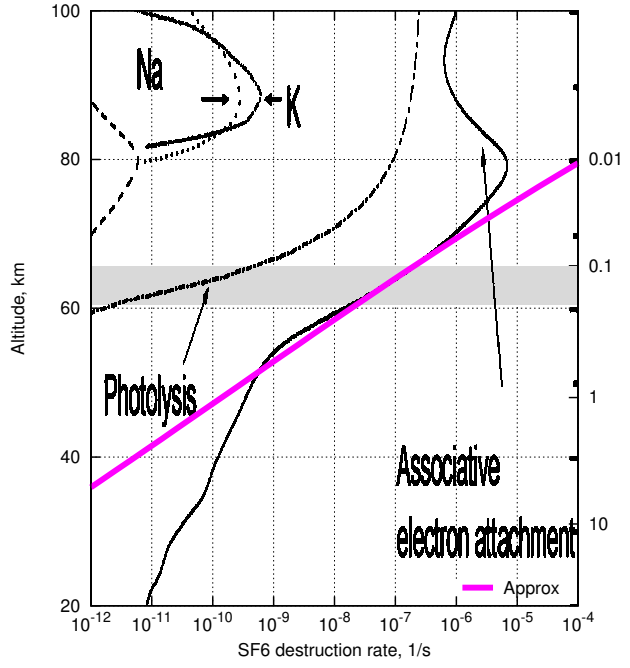

Figure 1. The vertical profiles of SF_6 destruction rate (after Totterdill et al., 2015) and its approximation in range of 55-75 km, given by Eq. (1).

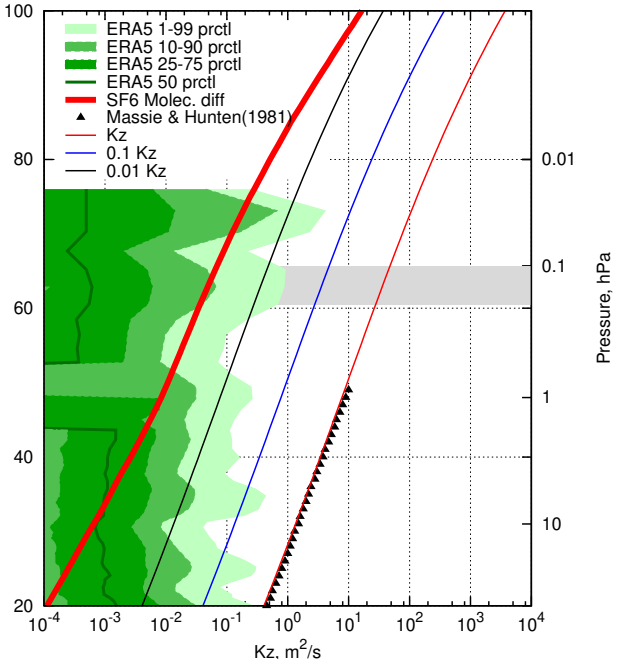

Figure 2. Vertical profiles of diffusion coefficients.

3 Silam developments

In this section we introduce a set of parametrizations implemented in Silam for this study.

3.1 SF_6 destruction

The destruction of atmospheric SF_6 occurs at altitudes over 60 km (Totterdill et al., 2015) that fall within the topmost layer of the ERA-Interim. The exchange processes in the upper stratosphere and lower mesosphere have to be adequately parameterized together with the destruction process.

Estimates of AoA from the SF_6 tracer rely on the assumption of it being a passive tracer. SF_6 is indeed essentially stable up to about 50 km altitudes. In the height range up to 100 km, the most pronounced destruction mechanism is associative electron attachment (Totterdill et al., 2015). The highest destruction rate of 10^{-5} s^{-1} occurs at the altitude of 80 km (Fig. 1). An important feature of this profile is that the destruction rate becomes significant above the top of our modelling domain (10 Pa, 65 km). The ERA-Interim meteorological fields have the uppermost level at 10 Pa and do not resolve a vertical structure of the atmosphere above that level. In order to assess the loss of SF_6 due to destruction we have to parameterise the combined

https://doi.org/10.5194/acp-2019-592
Preprint. Discussion started: 4 July 2019

Atmospheric Chemistry and Physics Discussions

effect of diffusion of SF_6 to the upper layers and its destruction there. Then the steady-state fluxes can be applied as the upper boundary condition to our simulations.

As an approximation to the vertical profile of the destruction rate in an altitude range of 50–80 km we have fitted a corresponding part of the curve in Fig. 9a of Totterdill et al. (2015) with a power function of pressure (magenta line in Fig. 1):

$$\frac{1}{\tau} = 3 \cdot 10^{-8} s^{-1} \left(\frac{20\,\mathrm{Pa}}{p} \right)^3, \tag{1}$$

where τ is the lifetime of SF_6 at the altitude corresponding to pressure p.

3.2 Eddy diffusivity

Large variety of vertical profiles for eddy diffusivity in the stratosphere and lower mesosphere can be found in literature. In many studies in 1970-s – 1980-s the vertical profiles were derived from observed tracer concentrations neglecting the mean transport. Most studies suggested that the vertical eddy diffusion has a minimum of 0.2-0.5 m^2/s (Pisso and Legras, 2008) at 15-20 km agreeing quite well to the ones derived from radar measurements in the range of 15-20 km Wilson (2004). Above that altitude K_z was suggested to gradually increases by about 1.5 orders of magnitude at 50 km due to breaking gravity waves (Lindzen, 1981).

The theoretical estimates of the effective exchange coefficients considering the layered and patchy structure of stratospheric turbulence suggest 0.5–2.5 m^2/s for the upper troposphere and 0.015–0.02 m^2/s for the lower stratosphere (Osman et al., 2016), which is about an order of magnitude lower than the estimates above.

The values of eddy exchange coefficient at heights of 10-20km estimated from high-resolution balloon temperature measurements (Gavrilov et al., 2005) are ~ 0.01 m^2/s with no noticeable vertical variation. It is not clear, however, how representative the derived values are for UTLS in general. We could not find any reliable observations of vertical diffusion in a range of 30-50 km.

The parameterisation for vertical eddy diffusivity above the boundary layer used in SILAM has been adapted from the IFS model of the European Centre for Medium-range Weather Forecasts (ECMWF, 2015). However, in the upper troposphere the predicted eddy diffusivity is nearly zero. For numerical reasons a lower limit of 0.01 m^2/s is set for K_z in SILAM. Our sensitivity tests have shown that long-term simulations are practically insensitive to this limit as long as it is low enough (see results and discussion). The modelled K_z in the stratosphere is practically always set to the limiting value with relatively rare peaks, mostly in UTLS. Such scheme essentially turns off turbulent diffusion in the stratosphere. Same is true for recent ERA5 reanalysis dataset (Copernicus Climate Change Service (C3S), 2017) that provides the values of K_z among other model-level fields: the eddy diffusion practically always falls below the molecular diffusivity limit (Fig. 2), which is about two of orders of magnitude lower than the estimates referenced above.

As a reference for this study, we took a tabulated profile of Hunten (1975), as it was quoted by Massie and Hunten (1981). The original profile covers the range up to 50 km, and the extrapolation up to 80 km matches well the theoretical estimates by (Lindzen, 1981) and by Allen et al. (1981). We approximate the profile as a function of pressure in the range of $100 - 0.01\,\mathrm{hPa}$

https://doi.org/10.5194/acp-2019-592
Preprint. Discussion started: 4 July 2019

Atmospheric Chemistry and Physics Discussions

(15 – 60 km):

$$K_z(p) = 8\,\mathrm{m}^2/\mathrm{s}\left(\frac{100\,\mathrm{Pa}}{p}\right)^{0.75}. \quad (2)$$

The approximated profile was stitched with the default Silam profile with a gradual transition within an altitude range of 10 – 15 km to keep the tropospheric dispersion intact. This profile gives values of K_z is 3 – 6 orders of magnitude higher than ones accepted in models (Fig. 2), and 1-2 orders of magnitude higher than more recent estimates (Legras et al., 2005). In order to cover the whole range of K_z, along with (2) we used two intermediate profiles whose upper part was scaled with factors 0.03 and 0.001 relative to the reference one. The three prescribed eddy-diffusivity profiles are hereinafter referred as "1Kz", "0.03Kz", and "0.001Kz" respectively. The dynamic eddy-diffusivity profile adopted from the ECMWF IFS model is referred to as "ECMWF Kz". In all simulations the parameterization of K_z in the troposphere is the same, and linear transition from the SILAM K_z to the tabulated one occurs in the altitude range of 10 – 15 km.

3.3 Molecular diffusivity and gravity separation

In tropospheric and stratospheric CTMs gaseous admixtures are transported as tracers, i.e. advection and turbulent mixing do not depend on a species properties, whereas the molecular diffusion is negligible. Models that cover mesosphere, such as WACCM (Smith et al., 2011), account for molecular diffusion explicitly. Since some of the K_z parametrizations above often result in values below the molecular diffusivity, the parametrization of molecular diffusion has been implemented in SILAM.

The molecular diffusivity of SF_6 in the air at temperature $T_0 = 300$ K and pressure $p_0 = 1000\,\mathrm{hPa}$, is $D_0 = 1 \times 10^{-5}\,\mathrm{m\,s}^{-2}$ (Marrero and Mason, 1972, Table 22). The diffusivity at a different temperature T and pressure p is given by:

$$D = D_0 \frac{p_0}{p}\left(\frac{T}{T_0}\right)^{3/2}, \quad (3)$$

see e.g. Cussler (1997). The vertical profile of molecular diffusivity in the US standard atmosphere (NOAA et al., 1976) is shown in (Fig. 2). Note that the value for the reference diffusivity of SF_6 used in this paper is about a half of the one used in simulations with WACCM by Kovács et al. (2017). The reason is that WACCM uses a universal parametrization (Smith et al., 2011, Eq. 7 there) for all compounds. That parametrization relies solely on molecular mass of a tracer and does not account for e.g. the molecule collision radius. The latter is about twice larger for SF_6 molecule than for most of stratospheric tracers. Thus, for this study we use the value from Marrero and Mason (1972), which results from fitting laboratory data for diffusion of SF_6 in the air.

The vertical diffusion transport velocity of admixture with number concentration $\tilde{n}$ and molecular mass $\tilde{\mu}$ in neutrally-stratified media is given by (Mange, 1957):

$$w = -D\left[\frac{1}{\tilde{\mu}}\frac{\partial\tilde{\mu}}{\partial z} + \left(\frac{\tilde{\mu}}{\mu} - 1\right)\frac{\mu g}{kT}\right], \quad (4)$$

where μ is molecular masses of air, g – acceleration due to gravity, k is the Boltzmann constant, and T is temperature. With ideal gas law $p = nkT$, in which p is pressure, and n is number concentration, and static law $dp/dz = -g\rho$, where $\rho = \mu n$ is

https://doi.org/10.5194/acp-2019-592
Preprint. Discussion started: 4 July 2019

Atmospheric Chemistry and Physics Discussions

the air density, the equation (4) can be reformulated in terms of the admixture mixing ratio $\xi = \tilde{n}/n$ and pressure. Then the vertical gradient of the equilibrium mixing ratio will be:

$$\frac{\partial \xi}{\partial p} = \left(\frac{\tilde{\mu}}{\mu} - 1\right)\frac{\xi}{p}. \tag{5}$$

It is non-zero for an admixture of a molecular mass different from one of the air. Integrating the gradient (5) over vertical, one can obtain that the equilibrium mixing ratios of the admixture at two layers are proportional to the corresponding pressures taken to the power of $\tilde{\mu}/\mu - 1$. For heavy admixtures, such as SF_6 ($\tilde{\mu} = 0.146$ kg/mole) the equilibrium gradient of a mixing ratio is substantial. For example, the difference of equilibrium mixing ratio of SF_6 in the atmosphere between 10 and 20 Pa is a factor of 16.

In most of the atmosphere, the effect of gravitational separation is insignificant due to overwhelming effect of other mixing mechanisms, whereas in the upper stratosphere the molecular diffusivity may become significant. Thus in the upper stratosphere heavy gases can no longer be considered as tracers and the molecular diffusion should be treated explicitly. The effect of gravitational separation of nitrogen and oxygen isotopes in the stratosphere has been observed (Ishidoya et al., 2008, 2013; Sugawara et al., 2018), however for isotopes the ratio of masses is relatively small, so the observed differences were also small (up to 10^{-5}). For SF_6 the molecular mass difference is much larger.

In order to enable the gravitational separation in SILAM we have introduced a molecular diffusion mechanism that can be enabled along with the turbulent vertical diffusion scheme. The exchange coefficients between the model layers are pre-calculated according to Eq. (4) discretised for the given layer structure for each species according to its diffusivity and molar mass. The US standard atmosphere (NOAA et al., 1976) was assumed for vertical profiles of temperature and air density during pre-calculation.

3.4 Parametrization for destruction of SF_6 in the mesosphere

As it has been mentioned above, the topmost level of the ERA-Interim meteorological data set is located at 10 Pa, which is below the layer where the destruction of SF_6 occurs. Therefore we have to put a boundary condition to our simulations to account for the upward flux of SF_6 through the upper boundary of the simulation domain. For that we assume that SF_6 distribution above the computational domain is in equilibrium with destruction and vertical flux.

Assuming the profiles for $K_z(p)$ and the SF_6 lifetime $\tau(p)$ are given by (2) and (1), one can obtain a steady-state distribution of mass-mixing ratio ξ of SF_6 due to destruction in the mesosphere at any point where both (2) and (1) are valid and vertical advection is negligible. This requires a solution of a steady-state diffusion equation with a sink:

$$\frac{\partial \xi}{\partial t} = g^2 \frac{\partial}{\partial p}\left(\rho^2 K_z(p)\frac{\partial \xi}{\partial p}\right) - \frac{\xi}{\tau(p)} = 0, \tag{6}$$

where $\rho(p)$ is air density, and g is acceleration due to gravity. Solving the Eq. (6) one can express the steady-state upward flux of SF_6 normalized with the mass mixing ratio at each pressure $\tilde{F}(p) = F(p)/\xi(p)$ as a function of p. The above equation was solved numerically with a boundary conditions of unit mixing ratio at a height of 100 Pa and vanishing flux at $p = 0$. Indeed

https://doi.org/10.5194/acp-2019-592
Preprint. Discussion started: 4 July 2019

Atmospheric Chemistry and Physics Discussions

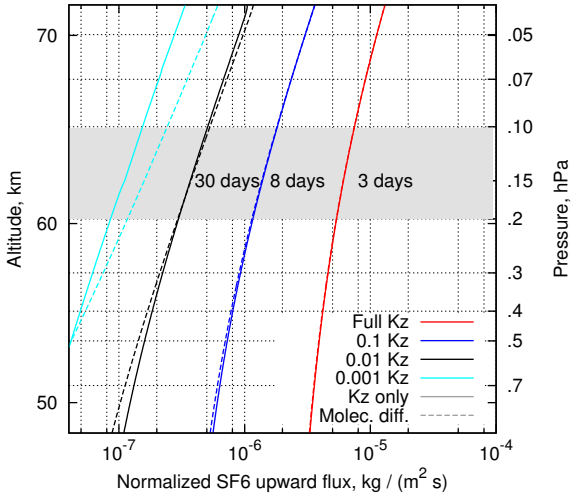

Figure 3. Vertical profiles of steady-state upward flux of SF_6 normalized with mass mixing ratio, for eddy diffusivity and lifetime profiles given by (2) and (1). The upper model layer of Silam and effective lifetimes of SF_6 there due to the destruction in the mesosphere for different K profiles are given.

for all considered cases the flux decreased by several orders of magnitude already at the level of a few Pa. The resulting $\tilde{F}(p)$ for four test profiles of K_z are shown in Fig. 3 with solid lines.

The effect of gravitational separation can be accounted for by introducing into Eq. (6) a term responsible for molecular diffusion and its equilibrium state (5):

$$\frac{\partial \xi}{\partial t} = g^2 \frac{\partial}{\partial p}\left(\rho^2 K_z(p)\frac{\partial \xi}{\partial p} + \rho^2 D(p)\left(\frac{\partial \xi}{\partial p} - \frac{\tilde{\mu}-\mu}{\mu}\frac{\xi}{p}\right)\right) - \frac{\xi}{\tau(p)} = 0. \tag{7}$$

The profiles of $\tilde{F}(p)$ resulting form this equation for SF_6 are given in Fig. 3 with dashed lines.

Accounting for molecular diffusion may either enhance or reduce the upward flux of SF_6 in the model. Along with setting the equilibrium state when the bulk of a heavy admixture is in the lower layers, molecular diffusion provides additional means for transport to the upper layers where the destruction occurs. For very low eddy diffusivities, the molecular diffusion is a sole mechanism of upward transport of SF_6 towards depletion layers. For higher eddy diffusivity the effect of molecular diffusion and gravitational separation becomes negligible.

For a model consisting of stacked well-mixed finite layers, the loss of SF_6 from the uppermost layer due to the steady upward flux would be proportional to the SF_6 mixing ratio in the layer. This loss of mass is equivalent to a linear decay of SF_6 in the layer at a rate $\tau^{-1} = g\tilde{F}(p)/\Delta p$, where Δp is a pressure drop in the layer.

For the upper layer of our simulations, the layer between 10 and 20 Pa (grey rectangle in Fig. 3) and $K_z(p)$ given with Eq. (2), the corresponding SF_6 lifetime τ in the layer is about 3 days. After scaling the $K_z(p)$ profile with factors of 0.1, 0.01, and 0.001 one gets the lifetimes of 8, 30, and 60 days respectively. Note that due to the molecular diffusion, the SF_6 lifetime in

https://doi.org/10.5194/acp-2019-592
Preprint. Discussion started: 4 July 2019


Atmospheric Chemistry and Physics Discussions

the topmost model layer becomes insensitive to the exact profile of the eddy diffusivity. In particular, for the considered layer it can not be longer than 60 days.

3.5 Simulation setup

The simulations of atmospheric transport were performed with the SILAM model for 1980-2018 years on a 1.44x1.44 degree global grid with 60 hybrid sigma-pressure layers starting from surface, with the uppermost layer between pressures of 20 and 10 Pa. The model time step of 15 minutes was been used and the output of daily mean concentrations of tracers together with air density was arranged.

The simulations were driven with ERA-interim meteorology at 0.72-degree resolution, so the meteorological input for both cell-interface for winds, and cell mid-points for other parameters was available without further interpolation. The gridded ERA-interim fields are, however, a result of reprojection of the original meteorological fields from spherical harmonics. Moreover, differences in the representation of model vertical structure between IFS and SILAM make a vertical reprojection necessary. These reprojections together with a limited precision of the gridded fields and inevitable small differences in physical parametrizations between IFS and SILAM result in inconsistency between surface-pressure tendencies and vertically-integrated air-mass fluxes calculated from the meteorological fields in SILAM. Such inconsistencies cause spurious variations in wind-field divergence that on long-term run result in accumulation of errors in tracer mixing ratios, and consequently, in the simulated AoA. Therefore, horizontal wind fields were adjusted by distributing the residuals of pressure tendency and vertically-integrated horizontal air-mass fluxes as a correction to the horizontal winds following the procedure suggested by Heimann and Keeling (1989). The correction is normally comparable to the precision of the input wind fields. The vertical wind component was then re-diagnosed from a divergence of horizontal air-mass fluxes for individual SILAM layers as described in Sofiev et al. (2015).

SILAM performs 3D transport by means of a dimension split: transport along each dimension is performed separately as 1D transport. To minimize the inconsistency between the tracer transport and air-mass fluxes, caused by the dimension split at finite time step, the splitting sequence has been inverted at each time step to reduce the accumulation of errors. The residual inconsistency was resolved by using a separate "ones" tracer, which was initialized to the constant mass mixing ratio of 1 at the beginning of a simulation. If advection was perfect, the concentration of "ones" would be equivalent to air density (mixing ratio would stay equal to 1). The mixing rations of simulated tracers were then evaluated as a ratio of a tracer mass in a cell to the mass of "ones".

In order to assess the effects of gravitational separation and destruction on the atmospheric distribution of SF_6, we have used four tracers: SF_6 as a passive tracer "sf6pass", SF_6 with gravitational separation but no destruction "sf6nochem" (no chemistry), SF_6 with destruction but no gravitational separation "sf6nograv", and SF_6 with both gravitational separation and destruction in the upper model level "sf6".

All SF_6 tracers had the same emission according to the SF_6 emission inventory (Rigby et al., 2010). The inventory covers 1970-2008, and was extrapolated with a linearly growing trend of $0.294\,\mathrm{Gg/y}$ until July 2016. The last 2.5 years were run without SF_6 emissions to evaluate its destruction rate.

https://doi.org/10.5194/acp-2019-592
Preprint. Discussion started: 4 July 2019

Atmospheric Chemistry and Physics Discussions

Besides the four SF_6 tracers we have used a "passive" tracer emitted uniformly at the surface at constant rate during the whole simulation time and an "ideal age" tracer. The "ideal age" tracer is defined as a tracer whose mixing ratio ξ_{ia} obeys continuity equation (Waugh, 2002):

$$\frac{\partial \xi_{ia}}{\partial t} + \mathcal{L}(\xi_{ia}) = 1, \tag{8}$$

(where $\mathcal{L}$ is an advection-diffusion operator), and boundary condition $\xi_{ia} = 0$ at the surface. The "ideal age" tracer is transported as a regular gaseous tracer, and to maintain consistency with other tracer mixing ratios, the ideal age is updated at every model time step Δt using the "ones" tracer:

$$M_{ia} \mapsto \begin{cases} 0, & \text{at lowest layer,} \\ M_{ia} + M_{ones}\Delta t, & \text{otherwise,} \end{cases} \tag{9}$$

where M_{ia} and M_{ones} are masses of "ideal age" tracer and of "ones" tracer in a grid cell. The mixing ratio of the "ideal age" tracer is a direct measure of the mean age of air in a cell, so the tracer is a direct Eulerian analogy of the time-tagged Lagrangian particles with clock reset at the surface.

A set of the simulations was performed with four settings for the eddy diffusivity profile, described in Sec. 3.2 and corresponding destruction rates of "sf6" and "sf6nograv" tracers in the uppermost model layer. All runs were initialized with the mixing ratios from the final state of a special initialization run performed with "0.001Kz" eddy diffusivity. The initialization simulation was started from zero fields for all tracers, except for "ones" tracer that was set to unity mixing ratio. The simulation was run with 1970-1979 emissions for SF_6 species, and driven by ERA-Interim meteorological fields for 1980-1989. The mixing ratios of all SF_6 tracers at the end of the initialization run were scaled to match the total SF_6 burden of 20.17 Gg in 1980 (Levin et al., 2010).

4 Sensitivity and validation of SF_6 simulations

4.1 Gravitational separation and mesospheric depletion

To evaluate the relative importance of gravitational separation and mesospheric depletion and their effect on the SF_6 concentrations we have compared the simulations for various SF_6 tracers and evaluated the relative reduction of SF_6 content in the stratosphere due to these processes. As a conservative estimate of the reduction, we evaluated the relative differences between the tracers in the latitude belt of 70-85S, since both processes have the most pronounced effect in southern polar vortex, where the downdraught of Brewer-Dobson circulation is the strongest.

Hereafter we quantify the effect of a relative difference between atmospheric contents of two SF_6 tracers "X" and "Y" defined as:

$$\Delta(\text{"X"}, \text{"Y"}) = 2\frac{\xi_X - \xi_Y}{\xi_X + \xi_Y} \cdot 100\% \tag{10}$$

https://doi.org/10.5194/acp-2019-592
Preprint. Discussion started: 4 July 2019

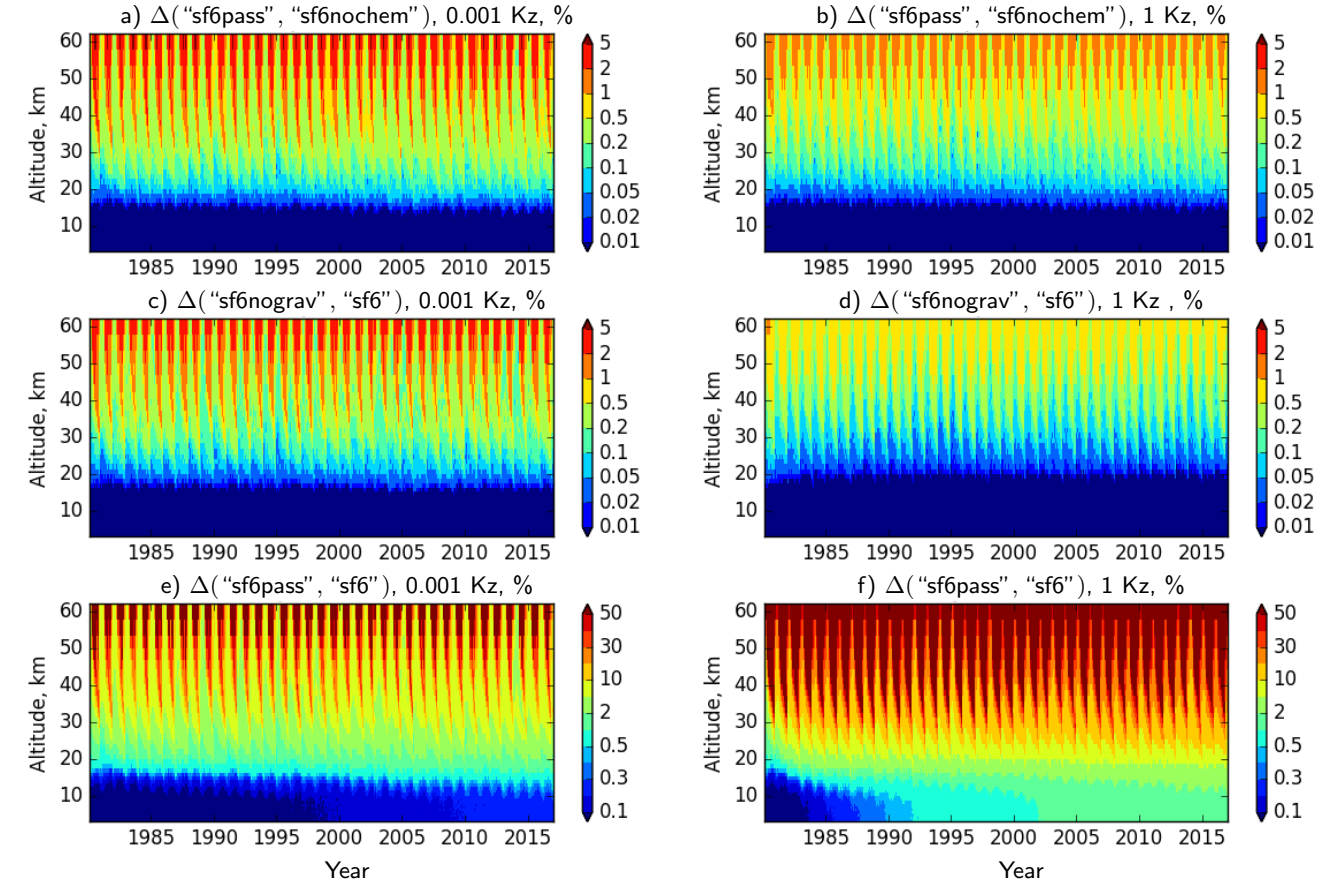

Figure 4. The relative reduction of SF_6 content (in %) at 70-85S due to gravitational separation with (a, b) and without (c, d) depletion, and due to combined effect of depletion and separation (e, f) at two extreme Kz cases. Note different color scales for e) and f).

The relative differences for the SF_6 tracers in the Southern polar region simulated with two extreme models for K_z is given in Fig. 4 as a function of time and altitude. Noteworthy, every 5% of decrease of SF_6 with respect to its passive counterpart correspond to about one year of a positive bias in AoA derived form SF_6 mixing ratios.

The reduction of SF_6 content due to gravitational separation if the mesospheric depletion is disabled is given by the relative difference of "sf6nochem" and "sf6pass" (Fig. 4ab). Expectedly, the effect of gravitational separation is most pronounced for the case of low eddy diffusivity ("0.001 Kz"), and the reduction of SF_6 in the altitude range of 30–50 km reaches 2 – 5 %. In the case of strong mixing, the effect of separation is about 1 %.

The reduction of SF_6 content due to gravitational separation in presence of stratospheric depletion given by the relative difference of "sf6nograv" and "sf6" tracers. The effect of the separation for low K_z is very similar between depletion and no-depletion case (Fig. 4c vs. Fig. 4a). Depletion reduces the effect of the gravitational separation for high K_z (Fig. 4b vs Fig. 4d).

https://doi.org/10.5194/acp-2019-592
Preprint. Discussion started: 4 July 2019

Atmospheric Chemistry and Physics Discussions

Tracer/ Kz scheme	removal rate, 10^3 mol/year	lifetime, years
passive, any Kz	0	∞
SF_6, ECMWF Kz	440	2900
SF_6, 0.001 Kz	480	2600
SF_6, 0.01 Kz	760	1700
SF_6, 0.03 Kz	800	1540
SF_6, 0.1 Kz	960	1300
SF_6, 1 Kz	2160	590

Table 1. SF_6 destruction rate after stopping emissions. Mid-2011 atmospheric burden of SF_6 of $1.27 \cdot 10^9$ moles is used as reference for the lifetime estimate

Regardless depletion, stronger K_z reduces the effect of the gravitational separation, however the latter is still non-negligible if precisions of order of a month for AoA are required.

.

The combined effect of depletion and gravitational separation is seen in the relative difference of "sf6pass" and "sf6" tracers (Fig. 4e and 4f). For both K_z cases the effect of depletion is by more than an order of magnitude stronger than one of gravity separation. Regardless the used K_z profiles, the reduction exceeds 50 %, which roughly corresponds to 10 years of an offset in the apparent AoA. The reduction has a noticeable inter-annual variability that poses substantial difficulties on applying a consistent correction to the apparent AoA. Contrary to the former two comparisons, stronger eddy mixing leads to stronger reduction of SF_6 since it intensifies the transport to the depletion layers, and thus enhances the depletion rate.

Since the simulations for different K_z have been initialized with the same state matching the total amount of SF_6, the simulations with "0.01 Kz" showed relaxation of the SF_6 vertical distribution during the first few years of the simulations. For "1 Kz" case (4f) the gradual increase of the difference between SF_6 and its passive version in the troposphere can be seen. The rate of this increase is about 0.5% per 39 years of simulations. This rate should not be confused with the depletion rate of SF_6 in the atmosphere since the difference is a combined effect of depletion and growth of emission rate, despite the latter is exactly the same for both tracers.

The above comparison indicates that the depletion has the stronger effect on the distribution of the SF_6 mixing ratio in the upper stratosphere than gravitational separation and molecular diffusion. However, the important role of the molecular diffusion is that it maintains the upward flux towards the mesosphere in the simulations even if the eddy diffusivity ceases.

Further in this paper only the "sf6pass" and "sf6' tracers will be used.

https://doi.org/10.5194/acp-2019-592
Preprint. Discussion started: 4 July 2019

Atmospheric Chemistry and Physics Discussions

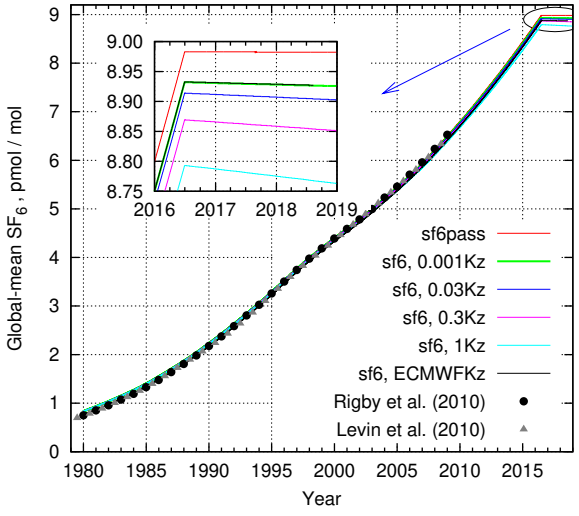

Figure 5. The time series of mean mixing ratio of SF_6 in the atmosphere simulated with emissions stopped in July 2016. The total burden by Levin et al. (2010) and by Rigby et al. (2010) are shown for comparison.

4.2 Lifetime of SF_6 in the atmosphere

In order to estimate the atmospheric lifetime of SF_6 we turned off the emission of all simulated SF_6 tracers in July 2016 and let the model run until the end of 2018 without emissions (Fig. 5). The decrease of the simulated SF_6 burden after the emission stop can be used to estimate the SF_6 removal rate from the atmosphere.

Time series of the total burden of SF_6 in the atmosphere in the simulations are given in Fig. 5. For easier comparison to observed mixing ratios the burden has been normalised with $1.78 \cdot 10^{20}$ moles – the total amount of air in the atmosphere – to get the mean mixing ratio. The tabulated values for the atmospheric burden of SF_6 from Levin et al. (2010) and Rigby et al. (2010) are given for comparison. Since the removal of SF_6 from the atmosphere is mostly controlled by the transport towards the depletion layer, the vertical exchange is a key controlling factor. In all simulated cases, the removal of SF_6 from the atmosphere is very slow, so the relative difference between the cases is small.

The decrease of the atmospheric SF_6 content after the emission stop, is given at the zoom panel of Fig. 5. As expected, after July 2016 the content of passive SF_6 stays constant, while depleting SF_6 start to fall down at a rate that depends on the transport properties of the stratosphere in the simulations, with faster removal for stronger eddy diffusivity. The removal rate is driven by the SF_6 content in the upper stratosphere, which is not in equilibrium with total atmospheric SF_6 content. A typical delay between SF_6 mixing ratio in the troposphere, where most of SF_6 resides, and the upper stratosphere, from where SF_6 escapes further to the depletion layers, is about 5-6 years. Hence, to estimate the SF_6 lifetimes we used the total amount of atmospheric SF_6 5 years before the emission stop, i.e. 1.23×10^9 mol, which corresponds to mean mixing ratio of about $7\,\mathrm{pmol/mol}$. Dividing the destruction rate with the reference amount one gets the range of corresponding simulated SF_6 life

https://doi.org/10.5194/acp-2019-592
Preprint. Discussion started: 4 July 2019

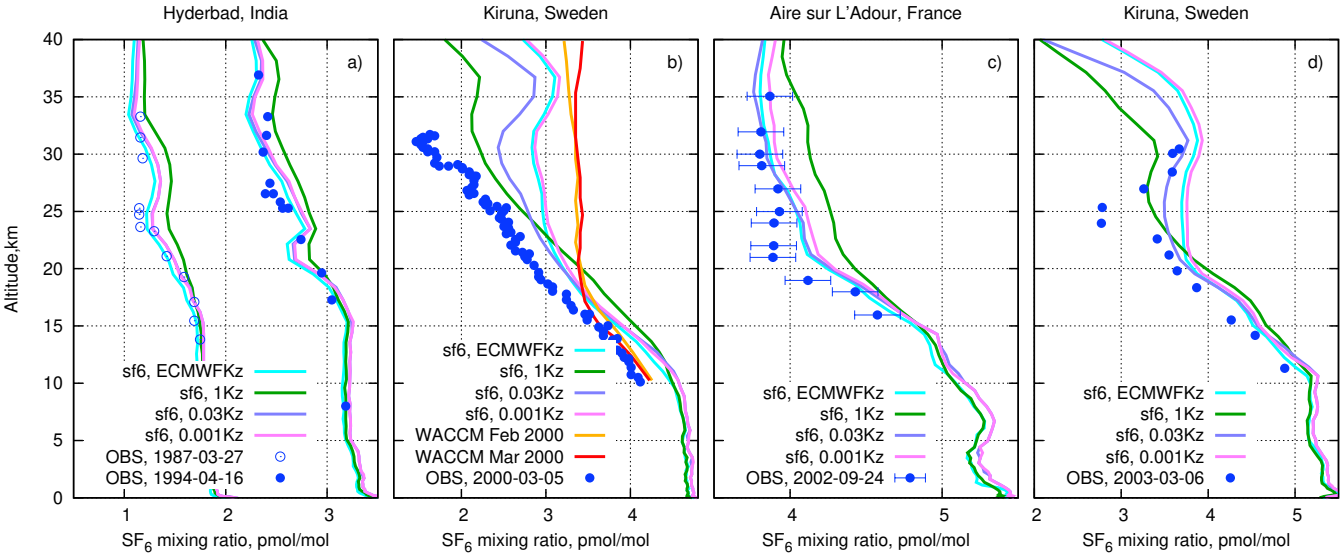

Figure 6. Observed SF_6 balloon profiles and corresponding daily-mean SILAM profiles for the date of observations. The observational data obtained from Patra et al. (1997), Ray et al. (2017), Ray et al. (2014), and Engel et al. (2006) for panels a–d correspondingly. The model profiles from WACCM model are from Ray et al. (2017).

times in the atmosphere: 600 to 2900 years. Despite the range of assumed diffusivities is three orders of magnitude, the decay rate of SF_6 varies only within a factor of five (Table 1).

The range of the SF_6 life times meets the ranges suggested by earlier studies. It is in a good agreement with results of Kovács et al. (2017), who obtained 1120 – 1475 years, and within the range of 800 – 3200 years, that one can find from model studies (Ravishankara et al., 1993; Morris et al., 1995), and 580–1400 years estimated from observational data (Ray et al., 2017).

4.3 Evaluation against balloon profiles

The tropospheric concentrations of SF_6 in our simulations have been practically insensitive to the way and rate of SF_6 destruction or to the choice of the eddy diffusivity profile. The difference in the modelled profiles can however be seen above the tropopause. For comparison we took the simulations with prescribed eddy diffusivity in stratosphere (1Kz, 0.03Kz, and 0.001Kz, see Sec. 3.2), and with dynamic eddy diffusivity "ECMWF Kz". The simulations were matched with stratospheric balloon observations we have found in a literature (Fig. 6).

Two balloon profiles observed at Hyderbad (17.5N,78.6E) in 1987 and 1994 by Patra et al. (1997) indicate an increase of SF_6 content during the time between the soundings (Fig. 6a). Both profiles have a clear transition layer from tropopause at ~ 17 km to undisturbed upper stratosphere above ~ 25 km. The simulated profiles agree quite well to the observed profiles, except for the most diffusive case that gave notably smoother profiles and somewhat overstated SF_6 mixing ratios due to too strong exchange through the tropopause.

https://doi.org/10.5194/acp-2019-592
Preprint. Discussion started: 4 July 2019


Atmospheric Chemistry and Physics Discussions

The profile in Fig. 6b has been obtained from Kiruna (68N, 21E) in early spring 2000 during the SAGE III Ozone Loss and Validation Experiment, SOLVE, (Ray et al., 2002) with the Lightweight Airborne Chromatograph (Moore et al., 2003). The profile is affected by the polar vortex and clearly indicates a strong reduction of SF_6 with height with a pronounced local minimum at 32 km. The corresponding SILAM profiles tend to overestimate the SF_6 vmr. The "ECMWF Kz" profile practically coincides to "0.001Kz", since vertical mixing is negligible in both cases. The most diffusive profile "1Kz" has the strongest depletion in the upper part, but the largest deviation from the observations below 20 km. The intermediate-diffusion profile ("0.03Kz") is almost as close to observations as the non-diffusive profile. Moreover, the "0.03Kz" profile has a minimum at the same altitude as the observed one, albeit the modelled minimum is substantially less deep.

For comparison, Fig. 6b also contains monthly-mean profiles from the WACCM simulations of Ray et al. (2014) along with the observation data. The WACCM profiles match very well the observations below 17 km, but turn nearly constant above, thus under-representing the depletion of SF_6 inside the polar vortex. Monthly-mean SILAM profiles (not shown) were much closer to plotted daily profiles than to monthly WACCM ones.

For the mid-latitude profile in Fig. 6c from Aire-sur-l'Adour, France (43.7N,0.3W), all SILAM profiles except for "1Kz" practically fall within the observational error bars provided together with the data by Ray et al. (2017). Similar to the Kiruna case in Fig. 6b, the SILAM profiles are much smoother than the observed ones and are unable to reproduce the sharp transition at 20 km.

Another profile from within the polar vortex (Fig. 6d) was observed at the same Kiruna site as one in Fig. 6b, but three years later. The observed profile also has a minimum that is much deeper than in the modelled profiles. Similar to the case in Fig. 6b, the "0.03Kz" profile is the only one that has a pronounced minimum at the same altitude as the observed one.

In all above cases, the "1Kz" profile is clearly far too diffusive and is an outlier that is furthermost from the observations. The "ECMWF Kz" profiles practically coincide to "0.001Kz", since vertical mixing is negligible in both cases. The "0.03Kz" profiles appear to be most realistic out of the four considered simulations: they are close to observed ones and have local minima at right altitudes for both Kiruna profiles.

4.4 Evaluation of SF_6 against MIPAS data

The MIPAS observations provide the richest observational dataset for stratospheric SF_6. However, each individual observation has a substantial noise error, which is noticeably larger than the difference between observation and any of the SILAM simulations. The largest diversity of the modelled SF_6 profiles was observed in polar regions, therefore below we show the mean profiles for each season in southern and northern polar areas. Besides that, we consider statistics of the model performance against MIPAS measurements in lower and upper stratosphere separately. For simplicity, we do not show the statistics for the "ECMWF Kz" runs, since it is very similar to one for "0.001Kz".

For the comparison, the daily mean model profiles have been collocated to the observed ones, and then, an averaging kernel of the corresponding MIPAS profile was applied to the SILAM profile. For the comparison we took only the data points with all the following criteria met:

https://doi.org/10.5194/acp-2019-592
Preprint. Discussion started: 4 July 2019

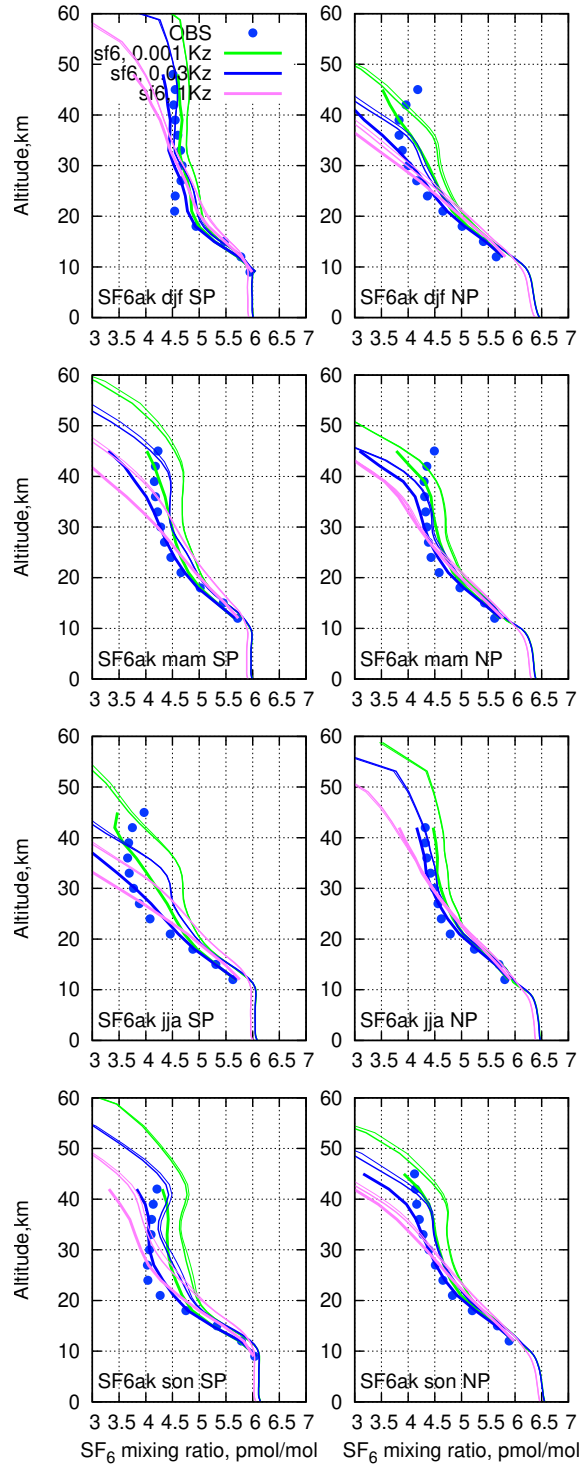

Figure 7. Seasonal mean collocated SILAM SF_6 and MIPAS profiles for 2007, for southern and northern polar regions

https://doi.org/10.5194/acp-2019-592
Preprint. Discussion started: 4 July 2019


Atmospheric Chemistry and Physics Discussions

- MIPAS visibility flag equals 1
- MIPAS Averaging kernel diagonal elements exceed 0.01
- MIPAS retrieval vertical resolution, i.e. full-width at half-maximum of the row of the averaging kernel, is better than $20\,\mathrm{km}$
- MIPAS volume mixing ratio noise error of SF_6 is less than $3\,\mathrm{pmol/mol}$

The mean seasonal profiles of the SF_6 mixing ratio for southern and northern polar regions derived from the MIPAS observations and SILAM simulations for 2007 are given in Fig. 7. In order to facilitate the comparison of our evaluation with earlier study by Kovács et al. (2017) we have chosen the same year and same layout of the panels as Fig. 3 there. The main differences between Kovács et al. (2017) and current evaluation are:

- We used averages of collocated model profiles (bold lines). The non-collocated seasonal- and area-mean model profiles are given with thin lines for comparison.
- we use a newer version of MIPAS SF_6 data with considerably larger values in the upper stratosphere, compared to the version that was used by Kovács et al. (2017).
- We do not put error bars for the observed data, since the statistical uncertainty of the averaged values in the scale of the plots is smaller than a data point size. In Kovács et al. (2017) the bars are standard deviations of the observed values, rather than uncertainties of the mean.
- We use 3-km vertical bins for the profiles to make the points in MIPAS profiles distinguishable

First of all, note a substantial difference between collocated and non-collocated model profiles. The difference is caused by uneven sampling of the atmosphere by the satellite both in space and time. In particular, MIPAS, being a polar-orbiting instrument, makes more profiles per unit area closer to a pole than further away. The difference gets somewhat reduced if one uses equal weights for all model grid cells instead of area-weighted averaging, especially for wide latitude belts. The major difference comes probably from the inability of MIPAS to retrieve SF_6 profiles in presence of polar stratospheric clouds that clutter lower layers of the stratosphere and make the sampling of polar regions quite uneven both in time and in vertical. This hypothesis agrees with fact that the difference is most pronounced for the winter pole, especially for the south pole in JJA, and practically negligible at a summer pole.

The comparison in Fig. 7 shows that the profiles from the SILAM simulations agree quite well to the observations in the altitude range below $20 - 25\,\mathrm{km}$, with the most diffusive "1Kz" slightly overstating the SF_6 mixing ratios. In the range above $25\,\mathrm{km}$, the '1Kz" profiles indicate too fast decrease of SF_6 with altitude. The "0.03Kz" profiles give the best results up to $\sim 40\,\mathrm{km}$, except for south pole in JJA and North pole in DJF.

None of the model setups is capable of reproducing adequately the observations above 40 km. Wintertime poles also pose a problem to the model. The disagreement indicates a deficiency in the model representation of air flows in the upper part of

https://doi.org/10.5194/acp-2019-592
Preprint. Discussion started: 4 July 2019

Atmospheric Chemistry and Physics Discussions

the domain caused by insufficient vertical resolution of ERA-Interim in the upper stratosphere and lower mesosphere, and lack of pole-to-pole circulation. This discrepancy is in line with the comparisons in Fig. 6 for polar regions. The model tends to overstate the SF_6 content in the lower part of a polar vortex, and understate it above $40\,\mathrm{km}$.

As more extensive verification of the SILAM simulations we computed statistical scores of the simulated SF_6 mixing ratios for each month of the MIPAS mission. The statistics were computed separately for the altitude range of 10 – $35\,\mathrm{km}$ (Fig. 8) and 30 – $60\,\mathrm{km}$ (Fig. 9). As the difference in statistical scores of the three selected simulations is quite minor, in addition to the aforementioned selection criteria for MIPAS data, we have selected only observations with the retrieval target noise error below $1\,\mathrm{pmol\,mol^{-1}}$.

The root-mean square error of is mostly controlled by the bias, and does not allow for clear distinction between the simulated cases. In order to disentangle the effect of bias, we have calculated the standard deviation of model-measurement difference (STD), absolute bias, and normalised mean bias. The latter is given by

$$\mathrm{NMB}(\%) = 2\left\langle \frac{M-O}{M+O} \right\rangle \cdot 100\%, \tag{11}$$

where M and O are modelled and observed values, respectively, and $\langle\cdot\rangle$ denotes averaging over the selected model-observation pairs for the given range of times and altitudes. Along with the STD, we have plotted the RMS error of the observations due to retrieval noise in the original MIPAS data.

In the altitude range of 10 – 35 km, the STD of model-measurement difference is practically uniform in time with minor peaks in August-September (Fig. 8). The level of the noise error constitutes about 85 % of the total model-measurement difference. Application of averaging kernel to the model profiles reduces the STD. The intermediate-diffusivity case "0.03Kz" clearly shows the least STD uniformly over the whole observation period, the same case indicates the least absolute bias.

In the range of 30 – 60 km altitudes (Fig. 9) the level of retrieval noise is noticeably higher than for the lower stratosphere. Unlike in the lower stratosphere, the least biased case is "1Kz", which has the largest STD. The STDs of "0.03Kz" and "0.001Kz" are practically on pair, however the latter has the strongest biases. Thus for the upper troposphere the intermediate-diffusivity case also shows the best performance.

5 Simulations of AoA

5.1 Eddy diffusivity and simulated AoA

The effect of the vertical eddy diffusivity on AoA in the stratosphere was evaluated with the same set of three prescribed K_z profiles and one dynamic K_z profile, as for SF_6 simulations. An example of annual-mean distributions of AoA for the same year is given in Fig. 10. The Hunten (1975) K_z profile (Fig. 10a) gives AoA in the stratosphere of about 3.5 years. It is much shorter than available estimates of stratospheric AoA (e.g. Waugh, 2009; Engel et al., 2009) from the observations of various tracers. Three other profiles of K_z result in practically identical distribution of AoA with typical stratospheric AoA of 5.5 years, which agrees quite well with the experimental estimates. Since "0.03Kz" profiles result in most realistic distribution of SF_6 in our simulations, in the current section we will use simulated distributions of tracers with "0.03Kz" eddy diffusivity.

https://doi.org/10.5194/acp-2019-592
Preprint. Discussion started: 4 July 2019

Atmospheric Chemistry and Physics Discussions

5.2 Age-of-Air and apparent SF_6 AoA

The constant-rate emission of the "passive" tracer in our simulations resulted in practically linear growth of the near-surface mixing ratio of the tracer after a decade of spin-up. The latter makes the age derived from the "passive" tracer equivalent to the age derived from the ideal-age tracer. The resulting distributions of "passive" and ideal-age AoA are indeed very close to each other (Fig. 11 a and b). The agreement confirms the self-consistency of the transport procedure since the tracers have opposite sensitivity to the advection errors: higher mixing ratios correspond to younger air for the accumulating tracers, while for the ideal-age tracer higher mixing ratios correspond to older air. The remaining differences are caused by spatial inhomogeneities of near-surface mixing ratio of "passive"due to variations in the near-surface air density.

The distribution of the AoA derived from "sf6pass" (Fig. 11c) is partly similar to the ideal-age one, however one can see substantial differences. The negative AoA in northern troposphere for the "sf6pass" tracer is caused by the predominant location of the sources in the northern hemisphere, so the concentrations there exceed global-mean levels. The growing rate of the SF_6 emissions leads to the greater than linear increase of near-surface mixing ratios, which leads to a slight old bias of the "sf6pass" AoA. This old bias has been one of the drawbacks of the SF_6 AoA pointed by Garcia et al. (2011).

The ages shown in Fig. 11a – c agree well with the ages derived from *in-situ* observations of SF_6 and CO_2 at the 25 km altitude by Waugh (2002). They also agree quite well with earlier simulations with five climate models that give annual mean ages in the upper stratosphere between 4.5 and 5.5 years (Butchart et al., 2010), and with Lagrangian simulations of (Diallo et al., 2012) driven by the same ERA-Interim meteorological fields as used for the present study. A substantial disagreement, however, exists with the ages derived from the MIPAS satellite observations (Stiller et al., 2012; Haenel et al., 2015), who calculated ages exceeding 10 years in polar areas and in the upper stratosphere. The reason for the disagreement follows from the above analysis: SF_6 can neither be considered as a passive tracer nor its mixing ration in the troposphere grows linearly with time. Denoting the AoA derived from the SF_6 profiles as "apparent AoA" (Waugh, 2002), we calculated it from the SILAM-predicted SF_6 profiles, which, as shown above, agree well well AoA derived from MIPAS. The resulting model-based apparent AoA (Fig. 11d) is indeed much older than the "ideal-age" AoA and pretty close to the values derived from MIPAS profiles by Stiller et al. (2012); Haenel et al. (2015).

The effect of apparent over-aging in the stratosphere due to the subsidence of the mesospheric air was estimated by Stiller et al. (2012) to be a fraction of a year in the upper stratosphere. In our simulations, the over-aging due to the SF_6 depletion and other factors discussed in previous sections is much stronger and affects practically the whole stratosphere. Recently Sugawara et al. (2018) also pointed that SF_6 AoA clearly deviates form AoA obtained from CO_2 already above 25 km.

5.3 Trends in apparent AoA

Changes in AoA have been used in many studies as an indicator of changes in the atmospheric circulation. In order to evaluate the effect of the way AoA is evaluated on trends in AoA we have calculated trends in apparent AoA at different altitudes and latitudes for 2002-2012. This period roughly covers the MIPAS mission time and allows for comparison with trends reported by Haenel et al. (2015).

https://doi.org/10.5194/acp-2019-592
Preprint. Discussion started: 4 July 2019

Atmospheric Chemistry and Physics Discussions

The zonal-mean vertical profiles of the AoA trends during 2002-2012 are shown in Fig. 12 for five latitudinal belts. The presented variable is a slope of the linear fit of the AoA time series for each tracer, averaged over the corresponding latitudinal belt and model layer. The fit was made with the ordinary least-squares method for each tracer. The error-bars show 95-% confidence intervals, calculated as if a model of linear trend with uncorrelated Gaussian noise was applicable to the time series.

The trends of the apparent AoA for the non-passive SF_6 species have a clear increase with height in the upper part of the profiles. The increase is the largest at high latitudes. Such a behaviour of trends agrees well with the AoA trends of Haenel et al. (2015, Fig. 7) obtained from the MIPAS observations. The over-aging due to the mesospheric depletion of SF_6 has been discussed and estimated by Haenel et al. (2015); Kovács et al. (2017). However, Fig. 12 shows that the mesospheric depletion of SF_6 also affects its trend: the over-aging increases with time. The reason is that depletion is proportional to the SF_6 load, which grows with time.

The apparent AoA derived with passive SF_6 tracer "sf6pass" indicates a negative trend of about 0.5 years/decade. The trend is caused by the temporal variation of SF_6 emissions. In order to get unbiased AoA estimate from a passive tracer, one needs the mixing ratio at the surface increasing linearly with time. A steady growth of emission rate at the surface leads to faster-than-linear increase of near-surface mixing ratio and, thus, low-bias of AoA since younger (i.e. more rich with SF_6) air gets more weight when two volumes of different age mix. According to the inventory (Levin et al., 2010) used in this study, the SF_6 emission rate was growing in 1997–2000 about twice slower than after 2005. Consequently, the negative bias of apparent AoA has increased resulting in negative trend if AoA in the stratosphere.

The AoA trends derived from the "ideal age" and "passive" tracers agree through the whole range of altitudes and latitudes indicating internal consistency of our simulations. The main common feature of the profiles is the negative tendency of about -0.5 year/decade in the altitude range of 15-30 km. We suspect it to be a feature of the non-uniformity of the ERA-Interim dataset, which was produced with assimilation of an inhomogeneous set of the observations. During that period, the amount of the assimilated data on the upper-air temperatures was by an order of magnitude higher than before 2000 and two orders of magnitude higher than after 2010 (Dee et al., 2011). It had a clear impact on the patterns of analysis increments in ERA-Interim and, consequently, on the predicted stratospheric circulation. Due to such inhomogeneities, ERA-Interim was not recommended for climatological studies. Therefore we do not draw any conclusion here on the actual trends of AoA but highlight that the trends of apparent AoA are completely determined by the method of its calculation.

6 Conclusions

Eulerian simulations of the tropospheric and stratospheric transport of several tracers were performed with SILAM model driven by ERA-Interim reanalysis for 1980-2018. The simulations included several species representing SF_6 under different assumptions, a passive tracer emitted uniformly at the surface, and an "ideal age" tracer directly comparable with Lagrangian simulations of a particle residence time. To our best knowledge this is the first systematic evaluation of AoA derived from several different tracers within the same simulation over several decades, combined with extensive evaluation against MIPAS and balloon SF_6 observations.

https://doi.org/10.5194/acp-2019-592
Preprint. Discussion started: 4 July 2019

Atmospheric Chemistry and Physics Discussions

Due to the limited vertical coverage and resolution of ERA-Interim in the upper stratosphere, the SILAM simulation domain had a lid at 10 Pa, which is below the altitude of the SF_6 destruction. In order to perform realistic simulations of SF_6 in our setup, the eddy diffusion in the upper stratosphere and lower mesosphere had to be parameterised, along with the mesospheric sink of SF_6.

A set of simulations with different parameterisations for the vertical eddy diffusion showed that published profiles derived with no account for advection (see e.g. Massie and Hunten, 1981, and references threrin) overestimate the eddy diffusivity. On other hand, the eddy-diffusivity profiles for scalars calculated from ERA-Interim fields according to the IFS procedures ECMWF (2015)), or readily available from ERA5 reanalysis, appear to be of no relevance for the upper stratosphere, since they fall below the molecular diffusivity. Evaluation of our simulations against satellite and balloon observations indicated that the best agreement between simulated and observed SF_6 mixing ratios is achieved for the tabulated eddy-diffusivity profile of Hunten (1975) scaled down with a factor of 30. It is not clear, however, if this conclusion is valid beyond the specific setup. Thus, the question on the importance and magnitude of the eddy diffusivity in the upper stratosphere and lower mesosphere remains open. Our simulations indicate that the diffusivities of 0.1 m/s^2 or less can be used in the upper stratosphere, until the molecular diffusivity takes over.

The mesospheric sink of SF_6 has a major impact on the mixing ratios above $20\,\mathrm{km}$. The depletion impact is especially strong in wintertime polar areas due to the downdraft within a polar vortex. The sensitivity tests have shown that molecular diffusion and gravitational separation of SF_6 are responsible for up to a few percent of further reduction in SF_6 mixing ratios in the upper stratosphere.

A good agreement of simulated SF_6 distribution to the MIPAS observations up to the altitudes of 30-40 km and to available balloon profiles was shown. The standard deviation between MIPAS and modelled SF_6 mixing rations is up to 80 % controlled by noise error of the satellite retrievals. The results of the comparison also underline the importance of accurate collocation of model and observed data in terms of space, time and vertical averaging of observed data.

The lifetime of SF_6 in the atmosphere estimated from the best-performing setup is about 1500 years, in a good agreement with previous studies.

Our simulations were able to reproduce both AoA obtained in other model studies, and apparent SF_6 AoA derived from MIPAS observations. Having all tracers within the same simulations we were able to trace the differences in the estimated AoA to the peculiarities of each tracer. A good agreement of passive-tracer and "ideal-age" AoA indicates a consistency of the simulations, since these two methods have opposite sign of sensitivity to errors of the transport scheme.

The mesospheric sink has severe implications on the AoA derived form SF_6. The apparent over-aging introduced by the sink is large and variable in space and season. Moreover, the over-aging due to the sink increases as the atmospheric burden of SF_6 grows. All this makes SF_6 unsuitable to infer AoA above $\sim 20\,\mathrm{km}$. Even in for the fully-passive SF_6 tracer there are deviations of apparent AoA from the "ideal-age" AoA caused by variable rate of the emissions. These deviations appear as long-term trends in the apparent AoA that differ from trends in the "ideal-age AoA", and have little relation to actual trends in the atmospheric circulation.

https://doi.org/10.5194/acp-2019-592
Preprint. Discussion started: 4 July 2019

Atmospheric Chemistry and Physics Discussions

Procedures used to derive AoA from observations of various tracers in the atmosphere are inevitably based on assumptions and idealisations that have limited and often unknown area of applicability. The resulting uncertainties in AoA are large enough to preclude the use of apparent AoA and its trends for evaluation of changes in atmospheric circulation or for validation of atmospheric models. Observations of the tracers themselves, however, have quite well quantified uncertainties, so direct comparisons of simulated tracers to the observed ones are a very promising means for the atmospheric model evaluation. AoA in turn is a convenient means for model inter-comparison if a protocol of AoA derivation is well specified.

Code and data availability. The SILAM source code as well as the simulation results used for this study are available from MS or RK on request. The MIPAS observational data available from GS on request. ERA-Interim and ERA5 reanalyses data sets are available from the European Center for Medium-range weather forecast http://www.ecmwf.int.

Author contributions. RK performed the simulations and data analyses, prepared text and illustrations. MS and JV inspired the study and helped with discussions on content and structure of the study. GS provided MIPAS data and wrote sections about MIPAS observations. All authors participated in the final preparation of the text.

Competing interests. The authors declare no competing interests.

Acknowledgements. The authors acknowledge the support of projects: EU FP7-MarcoPolo (ID: 606953), ESA-ATILA (contract no. 4000105828/12/F/MO and ASTREX of Academy of Finland (grant 139126).

The SF_6 and mean age-of-air distributions from MIPAS observations were generated within the project STI 210/5-3 of the CAWSES priority program, funded by the German Research Foundation (DFG), and the project BDCHANGE (01LG1221B), funded by the German Federal Ministry of Education and Research (BMBF) within the "ROMIC" program.

The authors are grateful to Viktoria Sofieva (Finnish Meteorological institute) for reading the manuscript and providing useful comments, to Florian Haenel and Michael Kiefer (Karlsruhe Institute of Technology) for technical assistance in handling MIPAS SF_6 data.

https://doi.org/10.5194/acp-2019-592
Preprint. Discussion started: 4 July 2019

Atmospheric Chemistry and Physics Discussions

References

Allen, M., Yung, Y. L., and Waters, J. W.: Vertical transport and photochemistry in the terrestrial mesosphere and lower thermosphere (50–120 km), J. Geophys. Res., 86, 3617–3627, https://doi.org/10.1029/JA086iA05p03617, 1981.

Andrews, A. E., Boering, K. A., Daube, B. C., Wofsy, S. C., Loewenstein, M., Jost, H., Podolske, J. R., Webster, C. R., Herman, R. L., Scott, D. C., and et al.: Mean ages of stratospheric air derived from in situ observations of CO2, CH4, and N2O, J. Geophys. Res., 106, 32 295–32 314, https://doi.org/10.1029/2001jd000465, 2001.

Bhandari, N., Lal, D., and Rama, D.: Stratospheric circulation studies based on natural and artificial radioactive tracer elements, Tellus, 18, 391–406, https://doi.org/10.1111/j.2153-3490.1966.tb00250.x, 1966.

Boering, K., Wofsy, S., Daube, B., Schneider, H., Loewenstein, M., Podolske, J., and Conway, T.: Stratospheric mean ages and transport rates from observations of carbon dioxide and nitrous oxide, Science, 274, 1340–1343, https://doi.org/10.1126/science.274.5291.1340, 1996.

Butchart, N., Cionni, I., Eyring, V., Shepherd, T. G., Waugh, D. W., Akiyoshi, H., Austin, J., Brühl, C., Chipperfield, M. P., Cordero, E., and et al.: Chemistry–Climate Model Simulations of Twenty-First Century Stratospheric Climate and Circulation Changes, J. Climate, 23, 5349–5374, https://doi.org/10.1175/2010jcli3404.1, 2010.

Copernicus Climate Change Service (C3S): ERA5: Fifth generation of ECMWF atmospheric reanalyses of the global climate, Copernicus Climate Change Service Climate Data Store (CDS), 2018, https://cds.climate.copernicus.eu/cdsapp#!/home, 2017.

Cussler, E. L.: Diffusion: Mass Transfer in Fluid Systems (Cambridge Series in Chemical Engineering), Cambridge University Press, 1997.

Dee, D. P., Uppala, S. M., Simmons, A. J., Berrisford, P., Poli, P., Kobayashi, S., Andrae, U., Balmaseda, M. A., Balsamo, G., Bauer, P., and et al.: The ERA-Interim reanalysis: configuration and performance of the data assimilation system, Q. J. Roy. Meteorol. Soc., 137, 553–597, https://doi.org/10.1002/qj.828, 2011.

Diallo, M., Legras, B., and Chédin, A.: Age of stratospheric air in the ERA-Interim, Atmos. Chem. Phys., 12, 12 133–12 154, https://doi.org/10.5194/acp-12-12133-2012, 2012.

ECMWF: IFS Documentation – Cy41r1, Part 4: Physical processes, Tech. rep., European Center for Medium-range Weather Forecasts, http://old.ecmwf.int/publications/library/do/references/list/151, 2015.

Eluszkiewicz, J., Hemler, R. S., Mahlman, J. D., Bruhwiler, L., and Takacs, L. L.: Sensitivity of Age-of-Air Calculations to the Choice of Advection Scheme, J. Atmos. Sci., 57, 3185–3201, https://doi.org/10.1175/1520-0469(2000)057<3185:SOAOAC>2.0.CO;2, 2000.

Engel, A., Möbius, T., Haase, H.-P., Bönisch, H., Wetter, T., Schmidt, U., Levin, I., Reddmann, T., Oelhaf, H., Wetzel, G., et al.: Observation of mesospheric air inside the arctic stratospheric polar vortex in early 2003, Atmospheric Chemistry and Physics, 6, 267–282, https://doi.org/1680-7324/acp/2006-6-267, 2006.

Engel, A., Möbius, T., Bönisch, H., Schmidt, U., Heinz, R., Levin, I., Atlas, E., Aoki, S., Nakazawa, T., Sugawara, S., and et al.: Age of stratospheric air unchanged within uncertainties over the past 30 years, Nature Geosci, 2, 28–31, https://doi.org/10.1038/ngeo388, 2009.

England, M. H.: The age of water and ventilation timescales in a global ocean model, Journal of Physical Oceanography, 25, 2756–2777, https://doi.org/10.1175/1520-0485(1995)025<2756:TAOWAV>2.0.CO;2, 1995.

Garcia, R. R., Randel, W. J., and Kinnison, D. E.: On the determination of age of air trends from atmospheric trace species, Journal of the Atmospheric Sciences, 68, 139–154, https://doi.org/10.1175/2010JAS3527.1, 2011.

Gavrilov, N. M., Luce, H., Crochet, M., Dalaudier, F., and Fukao, S.: Turbulence parameter estimations from high-resolution balloon temperature measurements of the MUTSI-2000 campaign, Annales Geophysicae, 23, 2401–2413, https://doi.org/10.5194/angeo-23-2401-2005, 2005.

https://doi.org/10.5194/acp-2019-592
Preprint. Discussion started: 4 July 2019

Atmospheric Chemistry and Physics Discussions

Haenel, F. J., Stiller, G. P., von Clarmann, T., Funke, B., Eckert, E., Glatthor, N., Grabowski, U., Kellmann, S., Kiefer, M., Linden, A., and Reddmann, T.: Reassessment of MIPAS age of air trends and variability, Atmospheric Chemistry and Physics Discussions, 15, 14 685–14 732, https://doi.org/10.5194/acpd-15-14685-2015, 2015.

Hall, T. M. and Plumb, R. A.: Age as a diagnostic of stratospheric transport, J. Geophys. Res., 99, 1059–1070, https://doi.org/10.1029/93JD03192, 1994.

Hall, T. M., Waugh, D. W., Boering, K. A., and Plumb, R. A.: Evaluation of transport in stratospheric models, Journal of Geophysical Research: Atmospheres, 104, 18 815–18 839, 1999.

Heimann, M. and Keeling, C. D.: A three-dimensional model of atmospheric CO_2 transport based on observed winds: 2. Model description and simulated tracer experiments, pp. 237–275, American Geophysical Union (AGU), https://doi.org/10.1029/GM055p0237, 1989.

Hunten, D. M.: Estimates of Stratospheric Pollution by an Analytic Model, Proceedings of the National Academy of Sciences of the United States of America, 72, 4711–4715, http://www.jstor.org/stable/65270, 1975.

Ishidoya, S., Sugawara, S., Morimoto, S., Aoki, S., and Nakazawa, T.: Gravitational separation of major atmospheric components of nitrogen and oxygen in the stratosphere, Geophysical Research Letters, 35, https://doi.org/10.1029/2007gl030456, 2008.

Ishidoya, S., Sugawara, S., Morimoto, S., Aoki, S., Nakazawa, T., Honda, H., and Murayama, S.: Gravitational separation in the stratosphere–a new indicator of atmospheric circulation, Atmospheric Chemistry and Physics, 13, 8787–8796, https://doi.org/10.5194/acp-13-8787-2013, 2013.

Jacob, D. J., Prather, M. J., Rasch, P. J., Shia, R.-L., Balkanski, Y. J., Beagley, S. R., Bergmann, D. J., Blackshear, W. T., Brown, M., Chiba, M., Chipperfield, M. P., de Grandpré, J., Dignon, J. E., Feichter, J., Genthon, C., Grose, W. L., Kasibhatla, P. S., Köhler, I., Kritz, M. A., Law, K., Penner, J. E., Ramonet, M., Reeves, C. E., Rotman, D. A., Stockwell, D. Z., Van Velthoven, P. F. J., Verver, G., Wild, O., Yang, H., and Zimmermann, P.: Evaluation and intercomparison of global atmospheric transport models using 222Rn and other short-lived tracers, Journal of Geophysical Research: Atmospheres, 102, 5953–5970, https://doi.org/10.1029/96JD02955, 1997.

Koch, D. and Rind, D.: Beryllium 10/beryllium 7 as a tracer of stratospheric transport, Journal of Geophysical Research: Atmospheres, 103, 3907–3917, https://doi.org/10.1029/97JD03117, 1998.

Kovács, T., Feng, W., Totterdill, A., Plane, J. M. C., Dhomse, S., Gómez-Martín, J. C., Stiller, G. P., Haenel, F. J., Smith, C., Forster, P. M., García, R. R., Marsh, D. R., and Chipperfield, M. P.: Determination of the atmospheric lifetime and global warming potential of sulfur hexafluoride using a three-dimensional model, Atmospheric Chemistry and Physics, 17, 883–898, https://doi.org/10.5194/acp-17-883-2017, 2017.

Krol, M., de Bruine, M., Killaars, L., Ouwersloot, H., Pozzer, A., Yin, Y., Chevallier, F., Bousquet, P., Patra, P., Belikov, D., Maksyutov, S., Dhomse, S., Feng, W., and Chipperfield, M. P.: Age of air as a diagnostic for transport timescales in global models, Geoosci. Model Devel., 11, 3109–3130, https://doi.org/10.5194/gmd-11-3109-2018, 2018.

Leedham Elvidge, E., Bönisch, H., Brenninkmeijer, C. A., Engel, A., Fraser, P. J., Gallacher, E., Langenfelds, R., Mühle, J., Oram, D. E., Ray, E. A., et al.: Evaluation of stratospheric age of air from CF_4, C_2F_6, C_3F_8, CHF_3, HFC-125, HFC-227ea and SF_6; implications for the calculations of halocarbon lifetimes, fractional release factors and ozone depletion potentials, Atmospheric Chemistry and Physics, 18, 3369–3385, https://doi.org/10.5194/acp-18-3369-2018, 2018.

Legras, B., Pisso, I., Berthet, G., and Lefèvre, F.: Variability of the Lagrangian turbulent diffusion in the lower stratosphere, Atmos. Chem. Phys., 5, 1605–1622, https://doi.org/10.5194/acp-5-1605-2005, 2005.

https://doi.org/10.5194/acp-2019-592
Preprint. Discussion started: 4 July 2019

Atmospheric Chemistry and Physics Discussions

Levin, I., Naegler, T., Heinz, R., Osusko, D., Cuevas, E., Engel, A., Ilmberger, J., Langenfelds, R. L., Neininger, B., Rohden, C. v., et al.: The global SF6 source inferred from long-term high precision atmospheric measurements and its comparison with emission inventories, Atmospheric Chemistry and Physics, 10, 2655–2662, https://doi.org/10.5194/acp-10-2655-2010, 2010.

Li, S. and Waugh, D. W.: Sensitivity of mean age and long-lived tracers to transport parameters in a two-dimensional model, Journal of Geophysical Research: Atmospheres, 104, 30 559–30 569, https://doi.org/10.1029/1999JD900913, 1999.

Lindzen, R. S.: Turbulence and stress owing to gravity wave and tidal breakdown, Journal of Geophysical Research: Oceans, 86, 9707–9714, https://doi.org/10.1029/JC086iC10p09707, 1981.

Mange, P.: The theory of molecular diffusion in the atmosphere, Journal of Geophysical Research, 62, 279–296, 1957.

Marrero, T. R. and Mason, E. A.: Gaseous diffusion coefficients, Journal of Physical and Chemical Reference Data, 1, 3–118, https://doi.org/10.1063/1.3253094, 1972.

Massie, S. T. and Hunten, D. M.: Stratospheric eddy diffusion coefficients from tracer data, J. Geophys. Res., 86, 9859–9867, https://doi.org/10.1029/jc086ic10p09859, 1981.

Monge-Sanz, B. M., Chipperfield, M. P., Dee, D. P., Simmons, A. J., and Uppala, S. M.: Improvements in the stratospheric transport achieved by a chemistry transport model with ECMWF (re)analyses: identifying effects and remaining challenges, Q. J. Roy. Meteorol. Soc., 139, 654–673, https://doi.org/10.1002/qj.1996, 2012.

Moore, F., Elkins, J., Ray, E., Dutton, G., Dunn, R., Fahey, D., McLaughlin, R., Thompson, T., Romashkin, P., Hurst, D., et al.: Balloonborne in situ gas chromatograph for measurements in the troposphere and stratosphere, Journal of Geophysical Research: Atmospheres, 108, https://doi.org/1029/2001JD000961, 2003.

Morris, R. A., Miller, T. M., Viggiano, A., Paulson, J. F., Solomon, S., and Reid, G.: Effects of electron and ion reactions on atmospheric lifetimes of fully fluorinated compounds, Journal of Geophysical Research: Atmospheres, 100, 1287–1294, 1995.

NOAA, NASA, and USAF: U.S. Standard Atmosphere, U.S. Governement Printing Office, Washington D.C., 1976.

Osman, M., Hocking, W., and Tarasick, D.: Parameterization of large-scale turbulent diffusion in the presence of both well-mixed and weakly mixed patchy layers, Journal of Atmospheric and Solar-Terrestrial Physics, 143-144, 14–36, https://doi.org/10.1016/j.jastp.2016.02.025, 2016.

Patra, P. K., Lal, S., Subbaraya, B., Jackman, C. H., and Rajaratnam, P.: Observed vertical profile of sulphur hexafluoride (SF6) and its atmospheric applications, Journal of Geophysical Research: Atmospheres, 102, 8855–8859, https://doi.org/10.1029/96JD03503, 1997.

Patra, P. K., Houweling, S., Krol, M., Bousquet, P., Belikov, D., Bergmann, D., Bian, H., Cameron-Smith, P., Chipperfield, M. P., Corbin, K., et al.: TransCom model simulations of CH 4 and related species: linking transport, surface flux and chemical loss with CH 4 variability in the troposphere and lower stratosphere, Atmospheric Chemistry and Physics, 11, 12 813–12 837, https://doi.org/10.5194/acp-11-12813-2011, 2011.

Pisso, I. and Legras, B.: Turbulent vertical diffusivity in the sub-tropical stratosphere, Atmos. Chem. Phys., 8, 697–707, https://doi.org/10.5194/acp-8-697-2008, 2008.

Ravishankara, A. R., Solomon, S., Turnipseed, A. A., and Warren, R. F.: Atmospheric lifetimes of long-lived halogenated species, Science, 259, 194–199, https://doi.org/10.1126/science.259.5092.194, 1993.

Ray, E. A., Moore, F. L., Elkins, J. W., Hurst, D. F., Romashkin, P. A., Dutton, G. S., and Fahey, D. W.: Descent and mixing in the 1999–2000 northern polar vortex inferred from in situ tracer measurements, Journal of Geophysical Research: Atmospheres, 107, https://doi.org/10.1029/2001JD000961, 2002.

https://doi.org/10.5194/acp-2019-592
Preprint. Discussion started: 4 July 2019

Atmospheric Chemistry and Physics Discussions

Ray, E. A., Moore, F. L., Rosenlof, K. H., Davis, S. M., Sweeney, C., Tans, P., Wang, T., Elkins, J. W., Bönisch, H., Engel, A., et al.: Improving stratospheric transport trend analysis based on SF6 and CO2 measurements, Journal of Geophysical Research: Atmospheres, 119, 14–110, https://doi.org/10.1002/2014JD021802, 2014.

Ray, E. A., Moore, F. L., Elkins, J. W., Rosenlof, K. H., Laube, J. C., Röckmann, T., Marsh, D. R., and Andrews, A. E.: Quantification of the SF6 lifetime based on mesospheric loss measured in the stratospheric polar vortex, Journal of Geophysical Research: Atmospheres, 122, 4626–4638, https://doi.org/10.1002/2016JD026198, 2017.

Remsberg, E. E.: Methane as a diagnostic tracer of changes in the Brewer-Dobson circulation of the stratosphere, Atmos. Chem. Phys., 15, 3739–3754, https://doi.org/10.5194/acp-15-3739-2015, 2015.

Rigby, M., Mühle, J., Miller, B. R., Prinn, R. G., Krummel, P. B., Steele, L. P., Fraser, P. J., Salameh, P. K., Harth, C. M., Weiss, R. F., and et al.: History of atmospheric SF6 from 1973 to 2008, Atmos. Chem. Phys., 10, 10 305–10 320, https://doi.org/10.5194/acp-10-10305-2010, 2010.

Smith, A. K., Garcia, R. R., Marsh, D. R., and Richter, J. H.: WACCM simulations of the mean circulation and trace species transport in the winter mesosphere, Journal of Geophysical Research: Atmospheres, 116, https://doi.org/10.1029/2011JD016083, 2011.

Sofiev, M., Vira, J., Kouznetsov, R., Prank, M., Soares, J., and Genikhovich, E.: Construction of the SILAM Eulerian atmospheric dispersion model based on the advection algorithm of Michael Galperin, Geoosci. Model Devel., 8, 3497–3522, https://doi.org/10.5194/gmd-8-3497-2015, 2015.

Stiller, G. P., von Clarmann, T., Höpfner, M., Glatthor, N., Grabowski, U., Kellmann, S., Kleinert, A., Linden, A., Milz, M., Reddmann, T., Steck, T., Fischer, H., Funke, B., López-Puertas, M., and Engel, A.: Global distribution of mean age of stratospheric air from MIPAS SF_6 measurements, Atmos. Chem. Phys., 8, 677–695, https://doi.org/10.5194/acp-8-677-2008, 2008.

Stiller, G. P., von Clarmann, T., Haenel, F., Funke, B., Glatthor, N., Grabowski, U., Kellmann, S., Kiefer, M., Linden, A., Lossow, S., and Lopez-Puertas, M.: Observed temporal evolution of global mean age of stratospheric air for the 2002 to 2010 period, Atmos. Chem. Phys., 12, 3311–3331, https://doi.org/10.5194/acp-12-3311-2012, 2012.

Sugawara, S., Ishidoya, S., Aoki, S., Morimoto, S., Nakazawa, T., Toyoda, S., Inai, Y., Hasebe, F., Ikeda, C., Honda, H., et al.: Age and gravitational separation of the stratospheric air over Indonesia, Atmospheric Chemistry and Physics, 18, 1819–1833, https://doi.org/10.5194/acp-18-1819-2018, 2018.

Thiele, G. and Sarmiento, J. L.: Tracer dating and ocean ventilation, Journal of Geophysical Research: Oceans, 95, 9377–9391, https://doi.org/10.1029/JC095iC06p09377, 1990.

Totterdill, A., Kovács, T., Gómez Martín, J. C., Feng, W., and Plane, J. M. C.: Mesospheric Removal of Very Long-Lived Greenhouse Gases SF6 and CFC-115 by Metal Reactions, Lyman-α Photolysis, and Electron Attachment, The Journal of Physical Chemistry A, 119, 2016–2025, https://doi.org/10.1021/jp5123344, 2015.

Varanasi, P., Li, Z., Nemtchinov, V., and Cherukuri, A.: Spectral absorption-coefficient data on HCFC-22 and SF_6 for remote-sensing applications, Journal of Quantitative Spectroscopy and Radiative Transfer, 52, 323–332, https://doi.org/10.1016/0022-4073(94)90162-7, 1994.

Waugh, D.: Age of stratospheric air: Theory, observations, and models, Reviews of Geophysics, 40, https://doi.org/10.1029/2000rg000101, 2002.

Waugh, D.: Atmospheric dynamics: The age of stratospheric air, Nature Geosci, 2, 14–16, https://doi.org/10.1038/ngeo397, 2009.

Wilson, R.: Turbulent diffusivity in the free atmosphere inferred from MST radar measurements: a review, Annales Gephysicae, 22, 3869–3887, https://doi.org/10.5194/angeo-22-3869-2004, 2004.

https://doi.org/10.5194/acp-2019-592
Preprint. Discussion started: 4 July 2019

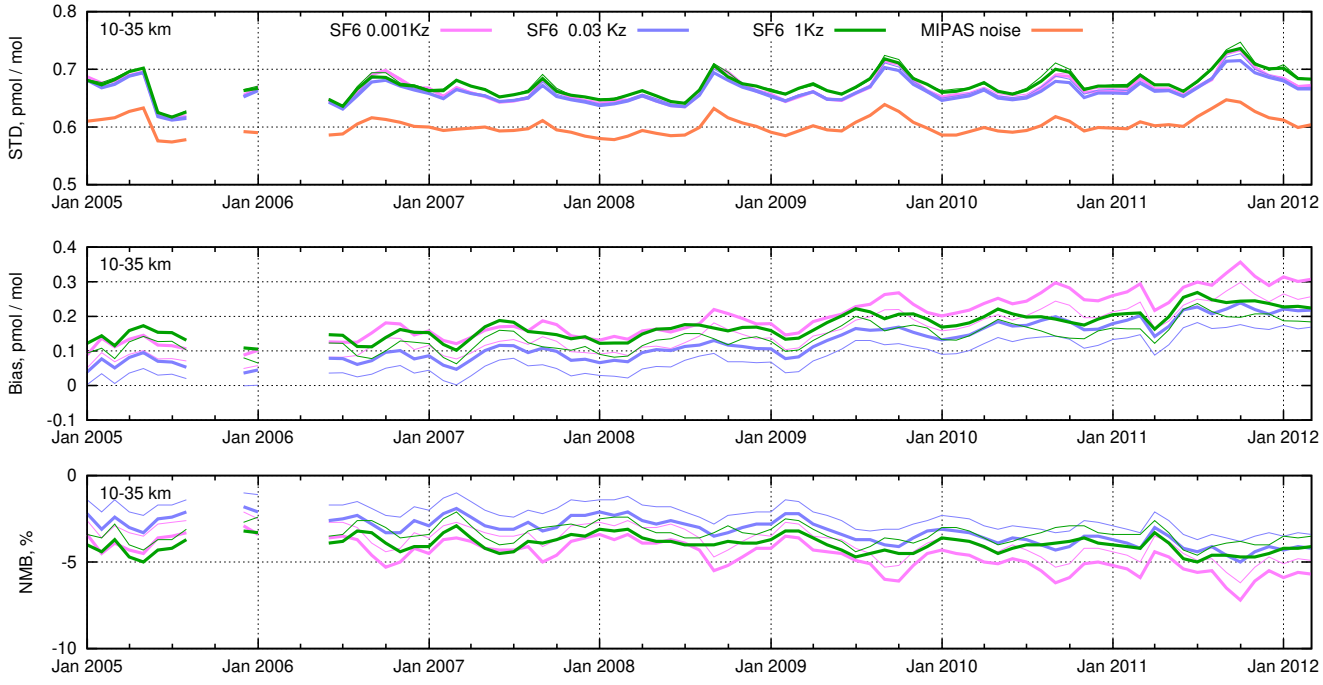

Figure 8. The time series of monthly scores for the SILAM-simulated SF_6 mixing ratios for the whole period of MIPAS observations in the altitude range of $10 - 35\,\mathrm{km}$. The statistics are: de-biased RMSE, absolute bias and normalised mean bias. The statistics of model mixing ratios extracted at nominal MIPAS altitudes are given in thin lines.

https://doi.org/10.5194/acp-2019-592
Preprint. Discussion started: 4 July 2019

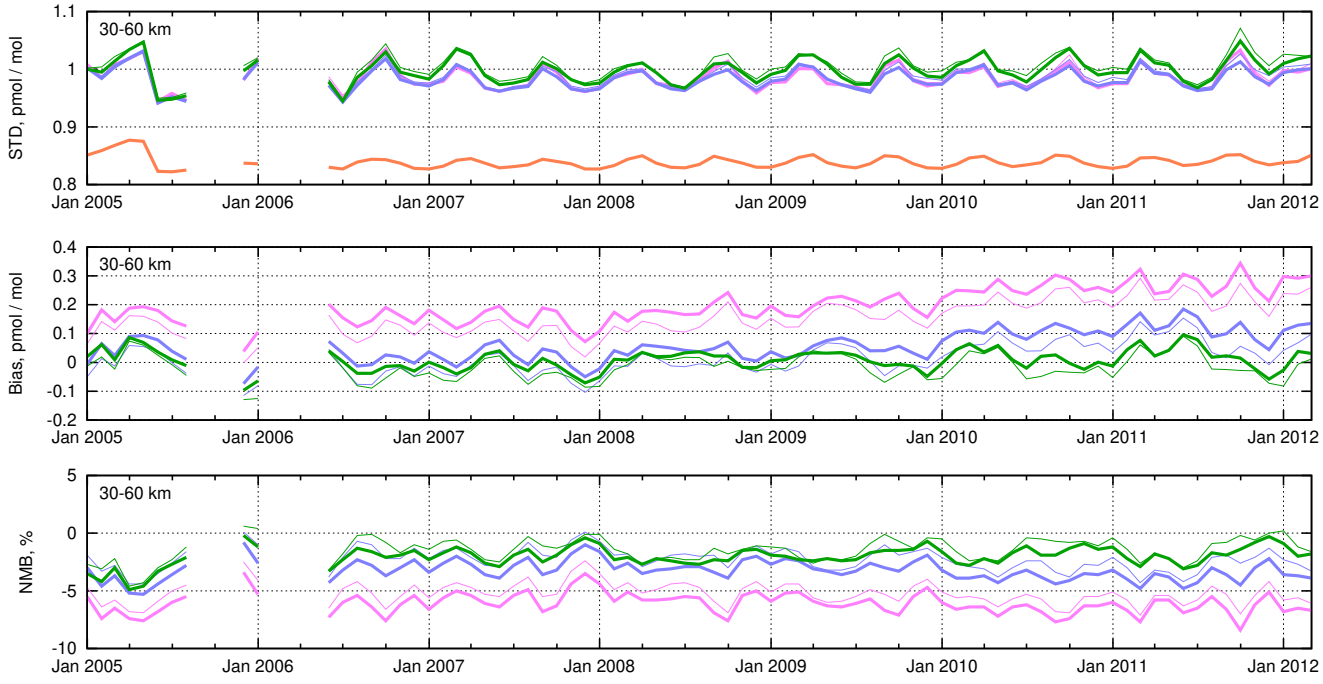

Figure 9. Same as in Fig. 8, but for the MIPAS altitude range of 30 – 60 km.

https://doi.org/10.5194/acp-2019-592
Preprint. Discussion started: 4 July 2019

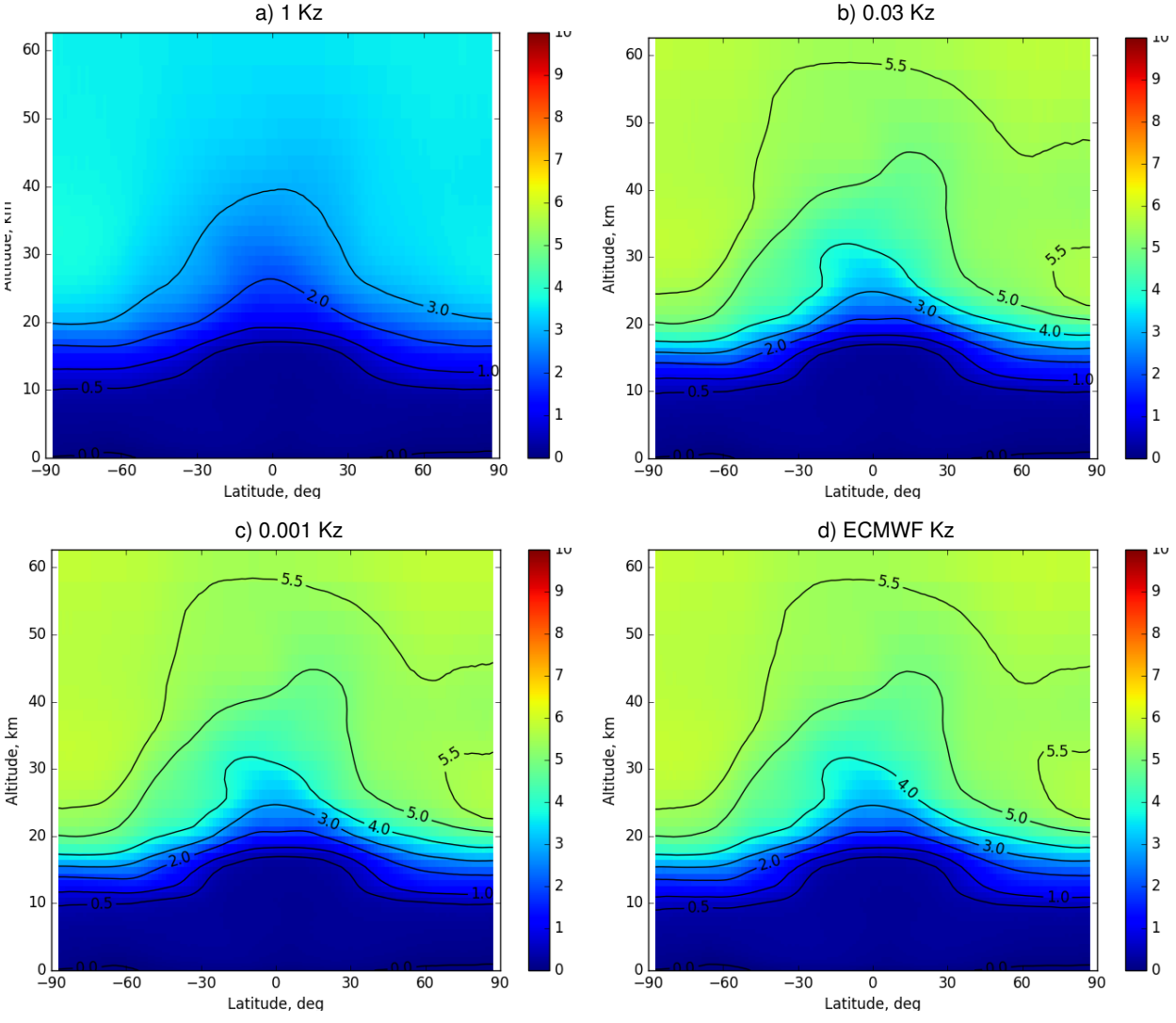

Figure 10. The zonal-mean spatial distribution of the ideal-age AoA for 2011 calculated for different eddy-diffusivity profiles.

https://doi.org/10.5194/acp-2019-592
Preprint. Discussion started: 4 July 2019

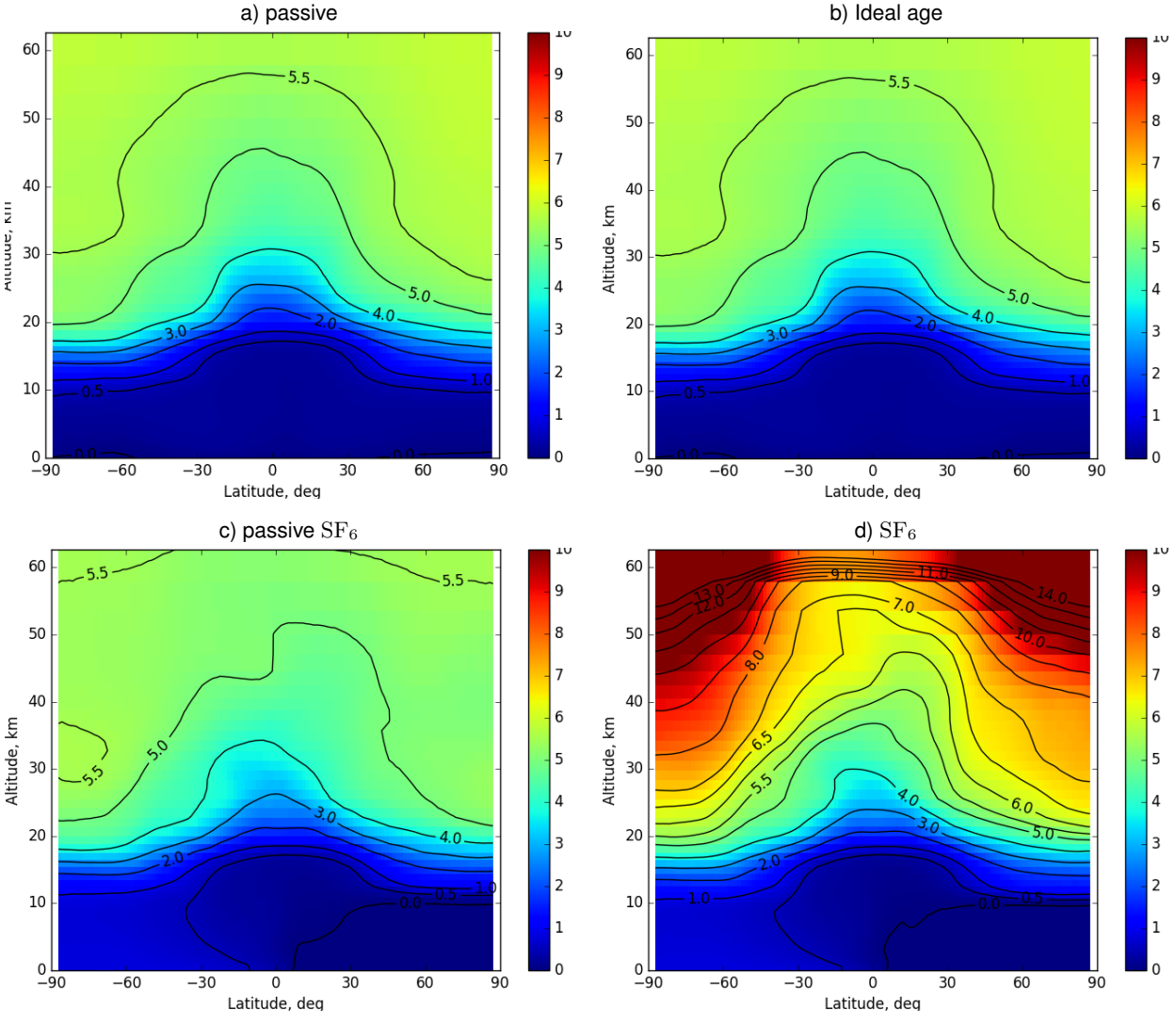

Figure 11. Zonal-mean distributions of atmospheric AoA simulated with "passive", ideal-age, and two SF_6 tracers, average for 2012.

https://doi.org/10.5194/acp-2019-592
Preprint. Discussion started: 4 July 2019

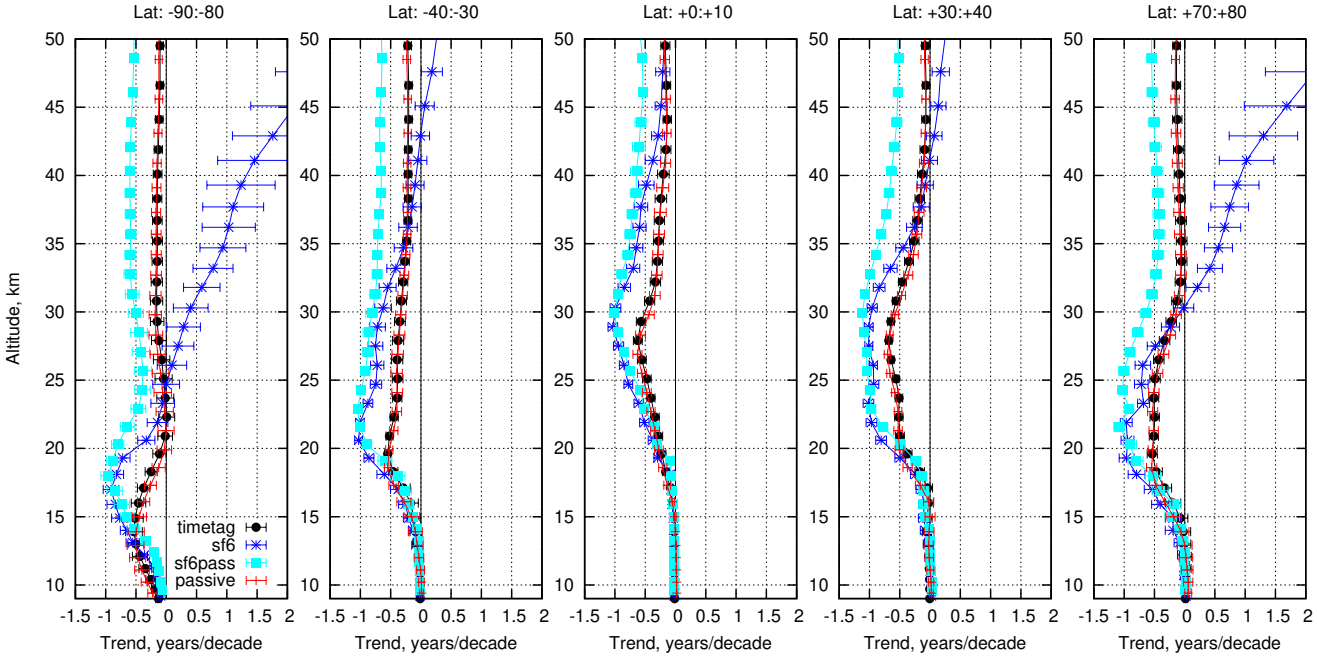

Figure 12. Vertical profiles of the simulated age of air linear trends over 2002-2012 for example latitude belts.